NEWTON, Volume *1*

Supplemental information

The role of magnetic dipolar interactions in skyrmion lattices

Elizabeth M. Jefremovas, Kilian Leutner, Miriam G. Fischer, Jorge Marqués-Marchán, Thomas B. Winkler, Agustina Asenjo, Jairo Sinova, Robert Frömter, and Mathias Kläui

Contents

Note S.1 SQUID magnetometry measurements

Figure S1 showcases the hysteresis loops (M *vs.* $\mu_0 H$) measured for out-of-plane (OOP) and in-plane (IP) geometries. Top panels **(A)** and **(B)** correspond to low repetition regime (n =1–4), while bottom figures **(C))** and **(D)** correspond to n = 10–30. The values for the saturation magnetization M_s, the effective anisotropy K_{eff}, and the uniaxial anisotropy K_{u}, defined as $K_{\mathrm{u}} = K_{\mathrm{eff}} + \mu_0 M_s^2/2$, are included in Table S 1. The increase the number of repetitions n does not trigger a spin reorientation transition, where the OOP magnetization would no longer be energetically favourable, and an easy-plane anisotropy, where the magnetization aligns within the plane, would be established. On the contrary, all our multilayer stacks remain with the magnetization OOP (PMA), where the saturation field of OOP saturation is well below the one of IP (up to $\approx$ 50 mT OOP, compared to $\approx$ 250 mT for IP saturation). Therefore, the effective anisotropy values calculated as the difference between the areas in-plane and out-of-plane, $K_{\mathrm{eff}} = A_{\mathrm{IP}} - A_{\mathrm{OOP}}$ stays positive across the whole range.

Table S 1: SQUID magnetometry data (M_s, K_{eff} and K_{u}) for the multilayer stacks. Errors indicated in brackets, affecting the last digit.

n	$\mathbf{M_s}$ (kA/m)	K_{eff} (kJ/m^3)	K_{u}**(kJ/m^3)**
1	610(20)	33(2)	270(30)
2	600(30)	62(5)	290(30)
3	630(30)	57(2)	320(20)
4	600(20)	74(7)	340(20)
10	600(10)	110	320(20)
12	600(20)	120(10)	340(20)
15	600(10)	140(10)	340(20)
18	600(30)	80(10)	300(40)
20	590(30)	90(10)	302(35)
25	600(30)	99(8)	315(40)
30	600(20)	110(10)	311(30)

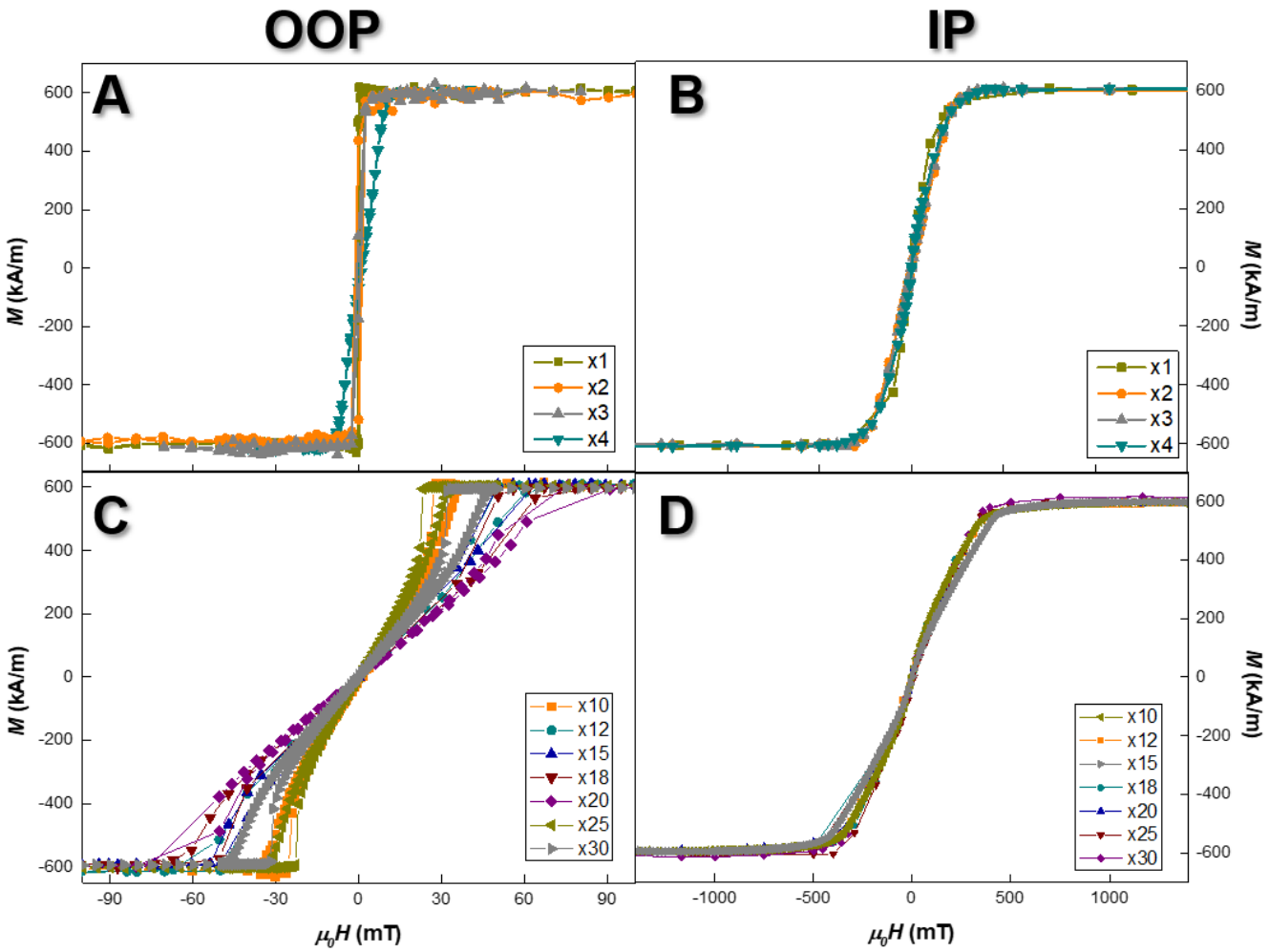

Figure S 1: M *vs.* $\mu_0 H$ hysteresis loops measured for: **(A)** and **(C)** out of plane (OOP); and **(B)** and **(D)** in–plane (IP) geometries.

Note S.2 Influence of the out-of-plane magnetic field on the skyrmion nucleation

The nucleation process of the skyrmion lattices requires from the combination of out-of-plane (OOP) + in-plane (IP) magnetic fields. As indicated in the main text, the IP component is in all cases larger than the OOP (we can estimate the OOP to be only around 15% the IP in the case of a 15° tilting). Therefore, the influence of the magnitude of the OOP component in the final skyrmion lattice can be concluded to be minor. However, in order to ascertain whether it influences the skyrmion size, or at all, the lattice density, we have tried to nucleate a series of skyrmion lattices modifying the OOP field magnitude.

Figure S2 includes a series of representative Kerr images for n = 2, where the magnitude of the OOP field is varied from 0.1 to 0.4 mT. As it can be observed, there is indeed an influence of the magnitude of the applied OOP field, as it needs to "fall within the skyrmion pockets": it needs to be sufficient to break completely the stripes (see Figure S2 **(A)**, with elongated stripes along the IP direction), but still below a certain threshold so as the skyrmion do not collapse back into maze-like OOP domains (see Figure S2**(D)**). However, in the intermediate situation, where the lattice is stabilized, there is no significant influence of the magnitude of the OOP field in the skyrmion size neither in the periodicity of the lattice (see 0.2 mT in Figure S2**(B)** and 0.3 mT in

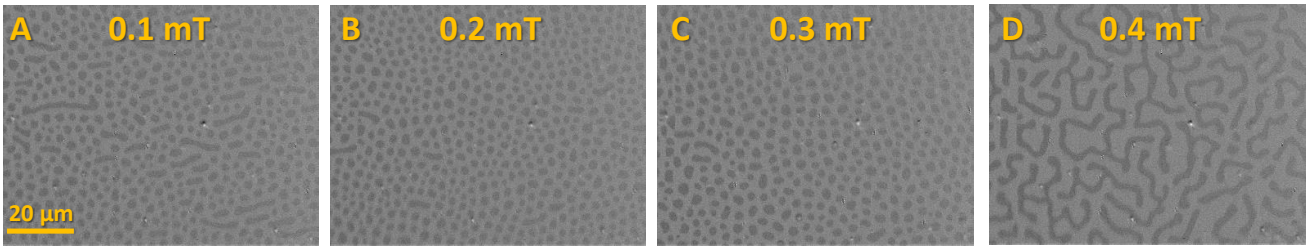

Figure S 2: Representative Kerr images for $n = 2$ stack after applying an OOP field of **(A)** 0.1, **(B)** 0.2, **(C)** 0.3 and **(D)** 0.4 mT, followed in all situations by an IP field of 120 mT.

Figure S2**(C)**). The lattice ground state is unique for each repetition, and it is independent from the OOP nucleation field used. The only guideline is that the OOP field needs to be within the range to nucleate skyrmion lattices. Once in this range, its magnitude does not affect significantly the skyrmion lattice, and the ground state is obtained.

Note S.3 Skyrmion lattice model

In the following, the theoretical model introduced in the main text of the paper will be derived. In addition to MuMax[3], Wolfram Mathematica[1], the Rubi package[2], Python 3, NumPy, and SciPy[3] were used.

3.1 Introduction

Our magnetic multilayer stack is treated using the effective medium model[4], where the whole stack is transformed into a single ferromagnetic layer. The total height of the stack is defined as $h = n_r h_{\mathrm{sr}}$, being $h_{\mathrm{sr}} = 4.92\,\mathrm{nm}$ the height of a single repetition. We refer the reader to Section Note S.4 for further justification of the effective medium model. The following material parameters are used:

$$M_s = 6 \times 10^5\,\mathrm{A\,m^{-1}}; A = 10 \times 10^{-12}\,\mathrm{J\,m^{-1}}; D = 0.9 \times 10^{-3}\,\mathrm{J\,m^{-2}}; K = 3 \times 10^5\,\mathrm{J\,m^{-3}}. \tag{3.1}$$

which, in the effective medium model, are transformed to:

$$M_s = 1.05 \times 10^5\,\mathrm{A\,m^{-1}}; A = 1.75 \times 10^{-12}\,\mathrm{J\,m^{-1}}; D = 1.57 \times 10^{-4}\,\mathrm{J\,m^{-2}}; K = 1.98 \times 10^4\,\mathrm{J\,m^{-3}}. \tag{3.2}$$

We consider skyrmions with radius R and domain wall width Δ, under the condition $R \gg \Delta$. The system is described by the x and y coordinates, which represent the in-plane coordinates of the magnetic film, and the z coordinate, which is perpendicular to the x and y coordinates. The skyrmions exist in an infinite film in the x and y directions, with finite height h in the z direction, *i.e.*, $\mathcal{V} = [-\infty, \infty] \times [-\infty, \infty] \times [0, h] = \mathbb{R}^2 \times [0, h]$. We further assume Néel skyrmions with a magnetization of $m_z = -1$ at their core, while the surrounding ferromagnetic film has $m_z = 1$.

3.1.1 Skyrmion lattice configurations

We consider the skyrmion centers located at $\vec{r} = i\vec{v}_1 + j\vec{v}_2$ with $(i, j) \in \mathbb{Z}^2$, where $\vec{v}_1, \vec{v}_2 \in \mathbb{R}^2$ are the lattice vectors. P is the periodicity of the skyrmion lattice. Additionally, we define ω as the two-dimensional region of the unit cell under consideration, with the corresponding three-dimensional volume given by:

$$\Omega = \{(x, y, z) \in \mathbb{R}^3 | (x, y) \in \omega, 0 \leq z \leq h\} \tag{3.3}$$

In this setting, we describe the two lattice configurations that are going to be considered in our work: square and hexagonal.

Square lattice For the square lattice, the vectors $\vec{v}_1$ and $\vec{v}_2$ are defined as:

$$\vec{v}_1 = P\vec{e}_x \qquad \vec{v}_2 = P\vec{e}_y. \tag{3.4}$$

The unit cell is given by:

$$\omega = \{(x, y) \in \mathbb{R}^2 | |x| \leq P/2, |y| \leq P/2\}. \tag{3.5}$$

The area of this unit cell is:

$$\mathrm{area}(\omega(P)) = P^2. \tag{3.6}$$

Hexagonal lattice For the hexagonal lattice, the lattice vectors are given by:

$$\vec{v}_1 = P\vec{e}_x \qquad \vec{v}_2 = P\left(\cos(120°)\vec{e}_x + \sin(120°)\vec{e}_y\right) = P\left(-\frac{1}{2}\vec{e}_x + \frac{\sqrt{3}}{2}\vec{e}_y\right), \tag{3.7}$$

and the unit cell ω under consideration is spanned by the vertices

$$\{(P/\sqrt{3}\cos(60°i - 30°), P/\sqrt{3}\sin(60°i - 30°))|i \in \{1,2,3,4,5,6\}\}. \tag{3.8}$$

The area of this unit cell is:

$$\text{area}(\omega(P)) = 6\left(\frac{1}{2}\cdot\frac{P}{2}\cdot\frac{P}{2}\tan\left(\frac{360°}{6}\cdot\frac{1}{2}\right)\right) = \frac{\sqrt{3}}{2}P^2. \tag{3.9}$$

The hexagonal lattice has a higher packing density than the square lattice. In Figure S 3, the hexagonal skyrmion lattice with ω, $\vec{v}_1$, and $\vec{v}_2$ is plotted.

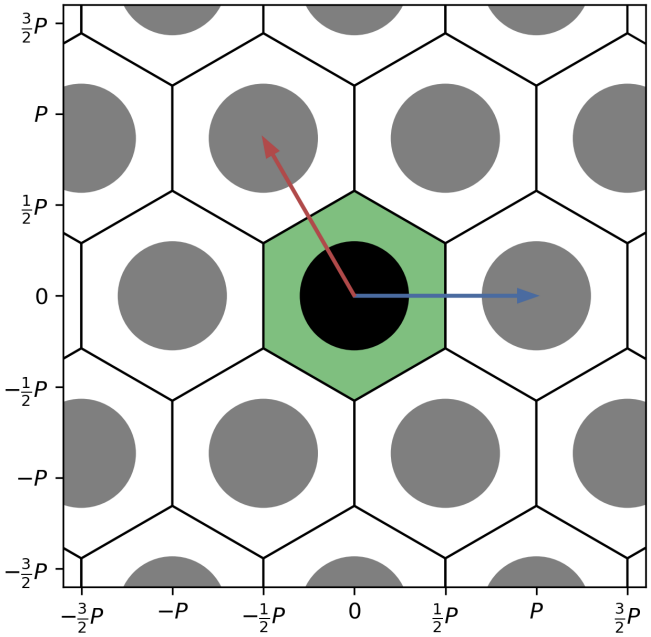

Figure S 3: The hexagonal skyrmion lattice is depicted, with the skyrmions shown in gray and black. The black lines mark the boundaries of the unit cells. The green background containing a skyrmion (black circle) indicates the considered unit cell ω. The blue vector is $\vec{v}_1$, and the red vector is $\vec{v}_2$.

3.1.2 Magnetization configuration of skyrmions $\vec{m}_\text{S}$ and the skyrmion lattice $\vec{m}_\text{L}$

The reduced magnetization, $\vec{m}_\text{S}(\vec{r})$, of an isolated Néel skyrmion with its center at $\vec{0}$ in an infinite ferromagnetic film can be described as follows[5–7]:

$$\vec{m}_\text{S}(r,\varphi) = \cos(\varphi)\sin(\theta(r))\vec{e}_x + \sin(\varphi)\sin(\theta(r))\vec{e}_y + \cos(\theta(r))\vec{e}_z, \tag{3.10}$$

where r is the radius and φ is the angle of the polar coordinates in the xy-plane, and $\theta(r)$ is the radial profile, given by:

$$\theta(r) = \frac{3\pi}{2} + \arcsin\left(\tanh\left(\frac{r-R}{\Delta}\right)\right). \tag{3.11}$$

$\theta(r)$ was chosen here in a simplified form that is valid in the limit $\Delta \ll R$. Additionally, $\sin(\theta(r)) = \operatorname{sech}\left(\frac{r-R}{\Delta}\right)$ and $\cos(\theta(r)) = \tanh\left(\frac{r-R}{\Delta}\right)$.

For the skyrmion lattice, with lattice vectors $\vec{v}_1$ and $\vec{v}_2$, the magnetization can be written as:

$$\vec{m}_{\mathrm{L}}(\vec{r}) = \vec{m}_{\mathrm{S}}(\vec{X}), \quad \vec{X} = \vec{r} - (\vec{v}_1 i + \vec{v}_2 j), \tag{3.12}$$

where (i, j) are determined by minimizing $|\vec{r} - (\vec{v}_1 i + \vec{v}_2 j)|$, such that i, j indicate the Wigner-Seitz cell in which $\vec{r}$ is located.

In the following sections, we will derive the energy terms necessary to describe skyrmion lattices

3.2 Exchange interaction E_{ex}

E_{ex} is the energy of the exchange interaction within a unit cell. Since the skyrmions (i.e., R) are smaller than a unit cell and skyrmion-skyrmion interactions are considered only via the magnetostatic field, the exchange energy E_{ex}, with exchange stiffness A, is given by[8]:

$$E_{\mathrm{ex}} = \int_{\Omega} \mathrm{d}^3\vec{r} \sum_{i,j\in\{x,y,z\}} (\partial_i(\vec{m}_{\mathrm{L}})_j)^2 = \int_{\mathcal{V}} \mathrm{d}^3\vec{r} \sum_{i,j\in\{x,y,z\}} (\partial_i(\vec{m}_{\mathrm{S}})_j)^2. \tag{3.13}$$

Rewritten in polar coordinates, this becomes:

$$E_{\mathrm{ex}} = A \int_{\mathcal{V}} \mathrm{d}^3\vec{r} \sum_{i,j\in\{x,y,z\}} (\partial_i(\vec{m}_{\mathrm{S}})_j)^2 = A\,h\,2\pi \int_0^{\infty} \mathrm{d}r\, r \left(\theta'(r)^2 + \frac{\sin^2(\theta(r))}{r^2}\right). \tag{3.14}$$

Since $R \gg \Delta$, the second term is negligible in good approximation, leading to:

$$E_{\mathrm{ex}} = A\,h\,2\pi \int_0^{\infty} \mathrm{d}r\, r\theta'(r)^2 = A\,h\,2\pi \log\left(1 + \exp\left(\frac{2R}{\Delta}\right)\right). \tag{3.15}$$

Given that $R \gg \Delta$, this simplifies to:

$$E_{\mathrm{ex}} = A\,2\pi R\,h\,\frac{2}{\Delta}. \tag{3.16}$$

3.3 Dzyaloshinskii–Moriya interaction E_{DMI}

Next, the energy of the interfacial isotropic Dzyaloshinskii–Moriya interaction within a unit cell, E_{DMI}, is considered. The energy E_{DMI}, with DMI interaction strength D, is given by[9]:

$$\begin{aligned} E_{\mathrm{DMI}} &= D \int_{\Omega} \mathrm{d}^3\vec{r} (\vec{m}_{\mathrm{L}})_x \partial_x(\vec{m}_{\mathrm{L}})_z + (\vec{m}_{\mathrm{L}})_y \partial_y(\vec{m}_{\mathrm{L}})_z - (\vec{m}_{\mathrm{L}})_z(\partial_x(\vec{m}_{\mathrm{L}})_x + \partial_y(\vec{m}_{\mathrm{L}})_y) \\ &= D \int_{\mathcal{V}} \mathrm{d}^3\vec{r} ((\vec{m}_{\mathrm{S}})_x \partial_x(\vec{m}_{\mathrm{S}})_z + (\vec{m}_{\mathrm{S}})_y \partial_y(\vec{m}_{\mathrm{S}})_z - (\vec{m}_{\mathrm{S}})_z(\partial_x(\vec{m}_{\mathrm{S}})_x + \partial_y(\vec{m}_{\mathrm{S}})_y) \\ &= -Dh\pi \int_0^{\infty} \mathrm{d}r\, \sin(2\theta(r)) + 2r\theta'(r). \end{aligned} \tag{3.17}$$

The same argument applies from the first to the second line as in the beginning of the exchange derivation (skyrmion smaller than the unit cell, skyrmion-skyrmion interactions considered via the

magnetostatic field). In the case $\Delta \ll R$, the first term can be neglected in a good approximation, resulting in:

$$\begin{aligned} E_{\mathrm{DMI}} &= -Dh\pi \int_0^\infty \mathrm{d}r\, 2r\theta'(r) \\ &= Dh\left(-4\pi r \arctan\left(e^{\frac{r-R}{\Delta}}\right) + 2i\pi\Delta\left(\mathrm{Li}_2\left(-ie^{\frac{r-R}{\Delta}}\right) - \mathrm{Li}_2\left(ie^{\frac{r-R}{\Delta}}\right)\right)\right). \end{aligned} \tag{3.18}$$

where $\mathrm{Li}_2(x)$ is the dilogarithm. In the limit $\Delta \ll R$, E_{DMI} simplifies to:

$$E_{\mathrm{DMI}} = -2\pi^2 D\, Rh. \tag{3.19}$$

3.4 Anisotropy E_{a}

The energy of the anisotropy interaction, E_{a}, in the considered unit cell, with the uniaxial anisotropy constant K, is given by[8]:

$$\begin{aligned} E_{\mathrm{a}} &= -K\int_\Omega \mathrm{d}^3\vec{r}(1-(\vec{m}_{\mathrm{L}})_z^2) = -K\int_{\mathcal{V}} \mathrm{d}^3\vec{r}(1-(\mathrm{m}_S)_z^2) \\ &= 2\pi Kh\int_0^\infty \mathrm{d}r\, r(1-\cos(\theta(r))^2) = K2h\Delta^2\pi\log\left(1+\exp\left(\frac{2R}{\Delta}\right)\right). \end{aligned} \tag{3.20}$$

The first term in the integrand is simply a constant energy that is added. For $\Delta \ll R$, the term can be well approximated by:

$$E_{\mathrm{a}} = K\, 2\pi R\, 2\Delta h. \tag{3.21}$$

3.5 Zeeman interaction E_{Z}

The Zeeman energy E_{Z} in the presence of a homogeneous field B_z within the considered unit cell is given by[8]:

$$E_{\mathrm{Z}} = -B_z M_s \int_\Omega \mathrm{d}^3\vec{r}\,[(\vec{m}_{\mathrm{L}})_z - 1] = -B_z M_s \int_{\mathcal{V}} \mathrm{d}^3\vec{r}\,[(\vec{m}_{\mathrm{S}})_z - 1]\,. \tag{3.22}$$

Here, the second term in the integral is a constant, ensuring a finite result. This leads to:

$$\begin{aligned} E_{\mathrm{Z}} &= 2\pi h B_z M_s \int_0^\infty \mathrm{d}r\ (1-\cos(\theta(r))) \\ &= -B_z M_s \Delta^2 \pi h\, \mathrm{Li}_2\left(-\exp\left(\frac{2R}{\Delta}\right)\right). \end{aligned} \tag{3.23}$$

In the limit $R \gg \Delta$, the Zeeman energy can be expanded as

$$E_{\mathrm{Z}} = B_z M_s 2\pi h R^2\left(1+\frac{\pi^2}{6}\left(\frac{\Delta}{R}\right)^2\right) \approx B_z 2\pi M_s h R^2. \tag{3.24}$$

3.6 Magnetostatic energy

3.6.1 Decomposition of terms

The magnetostatic energy for the considered unit cell, which arises both from the unit cell itself and from the surrounding lattice, is given by:

$$E_d = \frac{\mu_0}{8\pi}\left(\int_{\partial\Omega} \mathrm{d}^2\vec{r}'\,\sigma(\vec{r}') + \int_\Omega \mathrm{d}^3\vec{r}'\,\rho(\vec{r}')\right)\left(\int_{\partial\mathcal{V}} \mathrm{d}^2\vec{r}\,\sigma(\vec{r}) + \int_{\mathcal{V}} \mathrm{d}^3\vec{r}\,\rho(\vec{r})\right)\frac{1}{|\vec{r}-\vec{r}'|} \tag{3.25}$$

where the surface charges are $\sigma = \vec{n} \cdot \vec{M}$, the volume charges are $\rho = -\nabla \cdot \vec{M}$, and $\vec{M} = M_s \vec{m}_{\mathrm{L}}$.

The energy E_d can be decomposed into distinct contributions:

$$\begin{aligned} E_d &= E_{\sigma\rho} + E_{\sigma\sigma} + E_{\rho\rho} \\ E_{\sigma\rho} &= \frac{\mu_0}{8\pi} \int_{\partial\Omega} \mathrm{d}^2\vec{r}' \int_{\mathcal{V}} \mathrm{d}^3\vec{r} \frac{\sigma(\vec{r}')\rho(\vec{r})}{|\vec{r} - \vec{r}'|} + \frac{\mu_0}{8\pi} \int_{\partial\mathcal{V}} \mathrm{d}^2\vec{r}' \int_{\Omega} \mathrm{d}^3\vec{r} \frac{\sigma(\vec{r}')\rho(\vec{r})}{|\vec{r} - \vec{r}'|} \\ E_{\sigma\sigma} &= \frac{\mu_0}{8\pi} \int_{\partial\Omega} \mathrm{d}^2\vec{r}' \int_{\partial\mathcal{V}} \mathrm{d}^2\vec{r} \frac{\sigma(\vec{r}')\sigma(\vec{r})}{|\vec{r} - \vec{r}'|} \\ E_{\rho\rho} &= \frac{\mu_0}{8\pi} \int_{\Omega} \mathrm{d}^3\vec{r}' \int_{\mathcal{V}} \mathrm{d}^3\vec{r} \frac{\rho(\vec{r}')\rho(\vec{r})}{|\vec{r} - \vec{r}'|}. \end{aligned} \tag{3.26}$$

which are now being calculated.

3.6.2 Surface charge - volume charge interaction $E_{\sigma\rho}$

First, the surface charge - volume charge interaction $E_{\sigma\rho}$ is considered. With $\vec{r} = (x, y, z)$ and $\vec{r}' = (x', y', z')$, $E_{\sigma\rho}$ can be rewritten as:

$$\begin{aligned} E_{\sigma\rho} &= \frac{\mu_0}{8\pi} \int_{\partial\Omega} \mathrm{d}^2\vec{r}' \int_{\mathcal{V}} \mathrm{d}^3\vec{r} \frac{\sigma(\vec{r}')\rho(\vec{r})}{|\vec{r} - \vec{r}'|} + \frac{\mu_0}{8\pi} \int_{\partial\mathcal{V}} \mathrm{d}^2\vec{r}' \int_{\Omega} \mathrm{d}^3\vec{r} \frac{\sigma(\vec{r}')\rho(\vec{r})}{|\vec{r} - \vec{r}'|} \\ &= \frac{\mu_0}{8\pi} \int_{\omega} \mathrm{d}^2\vec{r}' \int_{\mathbb{R}^2} \mathrm{d}^2\vec{r} \int_0^h \mathrm{d}z \left(\frac{M(x', y', 0)\rho(x, y, z)}{\sqrt{(x - x')^2 + (y - y')^2 + z^2}} - \frac{M(x', y', h)\rho(x, y, z)}{\sqrt{(x - x')^2 + (y - y')^2 + (z - h)^2}} \right) \\ &+ \frac{\mu_0}{8\pi} \int_{\mathbb{R}^2} \mathrm{d}^2\vec{r}' \int_{\omega} \mathrm{d}^2\vec{r} \int_0^h \mathrm{d}z \left(\frac{M(x', y', 0)\rho(x, y, z)}{\sqrt{(x - x')^2 + (y - y')^2 + z^2}} - \frac{M(x', y', h)\rho(x, y, z)}{\sqrt{(x - x')^2 + (y - y')^2 + (z - h)^2}} \right). \end{aligned} \tag{3.27}$$

The following holds: $\forall z \in [0, h] : M_z(x, y, z) = M_z(x, y, 0)$, as the magnetization configuration of the skyrmion does not change along the z-axis. Therefore:

$$\begin{aligned} E_{\sigma\rho} = \frac{\mu_0}{8\pi} \int_{\omega} \mathrm{d}^2\vec{r}' \int_{\mathbb{R}^2} \mathrm{d}^2\vec{r} M(x', y', 0)\rho(x, y, 0) \int_0^h \mathrm{d}z \Bigg(& \frac{1}{\sqrt{(x - x')^2 + (y - y')^2 + z^2}} \\ & - \frac{1}{\sqrt{(x - x')^2 + (y - y')^2 + (z - h)^2}} \Bigg) \\ + \frac{\mu_0}{8\pi} \int_{\mathbb{R}^2} \mathrm{d}^2\vec{r}' \int_{\omega} \mathrm{d}^2\vec{r} M(x', y', 0)\rho(x, y, 0) \int_0^h \mathrm{d}z \Bigg(& \frac{1}{\sqrt{(x - x')^2 + (y - y')^2 + z^2}} \\ & - \frac{1}{\sqrt{(x - x')^2 + (y - y')^2 + (z - h)^2}} \Bigg). \end{aligned} \tag{3.28}$$

Together with the substitution $h - z = q$, the following holds:

$$\begin{aligned}
&\int_0^h \mathrm{d}z \frac{1}{\sqrt{(x-x')^2+(y-y')^2+z^2}} - \frac{1}{\sqrt{(x-x')^2+(y-y')^2+(z-h)^2}} \\
&= \int_0^h \mathrm{d}z \frac{1}{\sqrt{(x-x')^2+(y-y')^2+z^2}} - \int_h^0 \mathrm{d}q(-1) \frac{1}{\sqrt{(x-x')^2+(y-y')^2+q^2}} \\
&= \int_0^h \mathrm{d}z \frac{1}{\sqrt{(x-x')^2+(y-y')^2+z^2}} - \int_0^h \mathrm{d}q \frac{1}{\sqrt{(x-x')^2+(y-y')^2+q^2}} \\
&= 0.
\end{aligned} \tag{3.29}$$

Thus, the surface charge - volume charge interaction vanishes:

$$E_{\sigma\rho} = 0. \tag{3.30}$$

3.6.3 Decomposition of surface charges $E_{\sigma\sigma}$

The surface charge interaction is given by:

$$E_{\sigma\sigma} = \frac{\mu_0}{8\pi} \int_{\partial\Omega} \mathrm{d}^2\vec{r}' \int_{\partial\mathcal{V}} \mathrm{d}^2\vec{r} \frac{\sigma(\vec{r}')\sigma(\vec{r})}{|\vec{r}-\vec{r}'|} \tag{3.31}$$

and can be split into a term that describes the surface charge interaction of a ideal cylindrical lattice $E_{\sigma\sigma,\mathrm{c}}$, and a term that represents the deviation originating from a finite domain width Δ, represented by $E_{\sigma\sigma,\mathrm{nc}}$. Therefore, we can decompose:

$$\begin{aligned}
E_{\sigma\sigma} &= E_{\sigma\sigma,\mathrm{c}} + E_{\sigma\sigma,\mathrm{nc}} \\
E_{\sigma\sigma,\mathrm{c}} &= \lim_{\Delta\to 0} E_{\sigma\sigma} = \frac{\mu_0}{8\pi} \int_{\partial\Omega} \mathrm{d}^2\vec{r}' \int_{\partial\mathcal{V}} \mathrm{d}^2\vec{r} \frac{\sigma_{\Delta\to 0}(\vec{r}')\sigma_{\Delta\to 0}(\vec{r})}{|\vec{r}-\vec{r}'|} \\
E_{\sigma\sigma,\mathrm{nc}} &= E_{\sigma\sigma} - E_{\sigma\sigma,\mathrm{c}} = \frac{\mu_0}{8\pi} \int_{\partial\Omega} \mathrm{d}^2\vec{r}' \int_{\partial\mathcal{V}} \mathrm{d}^2\vec{r} \frac{\sigma(\vec{r}')\sigma(\vec{r}) - \sigma_{\Delta\to 0}(\vec{r}')\sigma_{\Delta\to 0}(\vec{r})}{|\vec{r}-\vec{r}'|}
\end{aligned} \tag{3.32}$$

where $\sigma_{\Delta\to 0} = M_s \lim_{\Delta\to 0} \vec{n} \cdot \vec{m}_{\mathrm{L}}$. Both terms, $E_{\sigma\sigma,\mathrm{c}}$ and $E_{\sigma\sigma,\mathrm{nc}}$, are now calculated.

3.6.4 Surface charge interaction of the cylindrical lattice $E_{\sigma\sigma,\mathrm{c}}$

Starting with the surface charge interaction of the cylindrical lattice $E_{\sigma\sigma,\mathrm{c}}$ can now be simplified as follows. The normal vector is $\vec{n} = \vec{e}_z$ for the top surface and $\vec{n} = -\vec{e}_z$ for the bottom surface, therefore:

$$\sigma_{\Delta\to 0}(\vec{r}') = M_s \lim_{\Delta\to 0} \vec{n} \cdot \vec{m}_{\mathrm{L}} = M_s (m_{L,\Delta\to 0})_z \in \{-M_s, M_s\}. \tag{3.33}$$

Thus, define a region for the surface of the cylinder as $\mathcal{R}_{\mathrm{c}}$, a region for the ferromagnetic background as $\mathcal{R}_{\mathrm{f}}$:

$$\begin{aligned}
\mathcal{R}_{\mathrm{c}} &= \{(x,y) \in \mathbb{R}^2 \,|\, \sigma_{\Delta\to 0}(x,y,h) = -M_s\} = \{\vec{v}_1 i + \vec{v}_2 j + \vec{r} \,|\, i,j \in \mathbb{Z},\, \vec{r} \in \mathbb{R}^2,\, |\vec{r}| \le R\} \\
\mathcal{R}_{\mathrm{f}} &= \{(x,y) \in \mathbb{R}^2 |\, \sigma_{\Delta\to 0}(x,y,h) = +M_s\} = \mathbb{R}^2 \setminus \mathcal{R}_{\mathrm{c}}.
\end{aligned} \tag{3.34}$$

We define the following function $g(A,B)$ which acts on arbitrary two dimensional regions:

$$g(A,B) = \frac{\mu_0 M_s^2}{8\pi} \int_A \mathrm{d}^2\vec{r}' \int_B \mathrm{d}^2\vec{r}\, 2\left(\frac{1}{|\vec{r}-\vec{r}'|} - \frac{1}{|\vec{r}-\vec{r}'+\vec{e}_z h|}\right), \tag{3.35}$$

With this it follows by superposition

$$\begin{aligned} E_{\sigma\sigma,\mathrm{c}} &= g(\omega\cap\mathcal{R}_\mathrm{c},\mathcal{R}_\mathrm{c}) + g(\omega\cap\mathcal{R}_\mathrm{f},\mathcal{R}_\mathrm{f}) - g(\omega\cap\mathcal{R}_\mathrm{f},\mathcal{R}_\mathrm{c}) - g(\omega\cap\mathcal{R}_\mathrm{c},\mathcal{R}_\mathrm{f}) \\ &= g(\omega,\mathbb{R}^2) - 4g(\omega\cap\mathcal{R}_\mathrm{c},\mathcal{R}_\mathrm{f}) \\ &= g(\omega,\mathbb{R}^2) - 4g(\omega\cap\mathcal{R}_\mathrm{c},\mathbb{R}^2) + 4g(\omega\cap\mathcal{R}_\mathrm{c},\mathcal{R}_\mathrm{c}). \end{aligned} \tag{3.36}$$

This can be rewritten as

$$E_{\sigma\sigma,\mathrm{c}} = E_\mathrm{f} + E_{\mathrm{c}\leftrightarrow\mathrm{f}} + E_\mathrm{c} + E_{\mathrm{c}\leftrightarrow\mathrm{c}}, \tag{3.37}$$

with

$$\begin{gathered} E_\mathrm{f} = g(\omega,\mathbb{R}^2) \quad E_{\mathrm{c}\leftrightarrow\mathrm{f}} = -4g(\omega\cap\mathcal{R}_\mathrm{c},\mathbb{R}^2) \\ E_\mathrm{c} + E_{\mathrm{c}\leftrightarrow\mathrm{c}} = 4g(\omega\cap\mathcal{R}_\mathrm{c},\mathcal{R}_\mathrm{c}) \quad E_\mathrm{c} = 4g(\omega\cap\mathcal{R}_\mathrm{c},\omega\cap\mathcal{R}_\mathrm{c}) \quad E_{\mathrm{c}\leftrightarrow\mathrm{c}} = 4g(\omega\cap\mathcal{R}_\mathrm{c},(\mathbb{R}^2\setminus\omega)\cap\mathcal{R}_\mathrm{c}). \end{gathered} \tag{3.38}$$

where E_f is the self-energy contribution of the film within the considered unit-cell ω, $E_{\mathrm{c}\leftrightarrow\mathrm{f}}$ represents the interaction between the cylinder and the film, E_c is the self-energy of the cylinder, and $E_{\mathrm{c}\leftrightarrow\mathrm{c}}$ describes the interaction between the cylinder in the considered unit cell and all the other cylinders in the cylinder lattice. This decomposition can be found using a related approach in Ref. 10.

Self-energy contribution of the film within the considered unit-cell E_f Using the divergence theorem and $\Delta_{\vec{r}}\frac{1}{4\pi|\vec{r}-\vec{r}_0|} = -\delta(\vec{r}-\vec{r}_0)$, the following holds for E_f:

$$\begin{aligned} E_\mathrm{f} = g(\omega,\mathbb{R}^2) &= \frac{\mu_0 M_s^2}{8\pi}\int_{\partial\Omega}\mathrm{d}^2\vec{r}'\int_{\partial\mathcal{V}}\mathrm{d}^2\vec{r}\,\frac{(\vec{n}_{\vec{r}'}\cdot\vec{e}_z)(\vec{n}_{\vec{r}}\cdot\vec{e}_z)}{|\vec{r}-\vec{r}'|} = -\frac{\mu_0 M_s^2}{8\pi}\int_\Omega\mathrm{d}^3\vec{r}'\int_\mathcal{V}\mathrm{d}^3\vec{r}\,\partial_z^2\left(\frac{1}{|\vec{r}-\vec{r}'|}\right) \\ &\text{since}\int_{\partial\Omega}\mathrm{d}^2\vec{r}'\int_{\partial\mathcal{V}}\mathrm{d}^2\vec{r}\,\frac{(\vec{n}_{\vec{r}'}\cdot\vec{e}_x)(\vec{n}_{\vec{r}}\cdot\vec{e}_x)+(\vec{n}_{\vec{r}'}\cdot\vec{e}_y)(\vec{n}_{\vec{r}}\cdot\vec{e}_y)}{|\vec{r}-\vec{r}'|} = 0 \\ &= -\frac{\mu_0 M_s^2}{8\pi}\int_\Omega\mathrm{d}^3\vec{r}'\int_\mathcal{V}\mathrm{d}^3\vec{r}\,\Delta_{\vec{r}}\left(\frac{1}{|\vec{r}-\vec{r}'|}\right) = \frac{\mu_0 M_s^2}{2}\int_\Omega\mathrm{d}^3\vec{r}'\int_\mathcal{V}\mathrm{d}^3\vec{r}\,\delta(\vec{r}-\vec{r}') \\ &= \frac{\mu_0 M_s^2}{2} h\,\mathrm{area}(\omega). \end{aligned} \tag{3.39}$$

Energy of interaction between the cylinder and the film $E_{\mathrm{c}\leftrightarrow\mathrm{f}}$ For $E_{\mathrm{c}\leftrightarrow\mathrm{f}}$, using the same arguments, one obtains:

$$\begin{aligned} E_{\mathrm{c}\leftrightarrow\mathrm{f}} = -4g(\omega\cap\mathcal{R}_\mathrm{c},\mathbb{R}^2) &= -\frac{\mu_0 M_s^2}{2\pi}\int_{\partial(\Omega\cap\mathcal{R}_\mathrm{c})}\mathrm{d}^2\vec{r}'\int_{\partial\mathcal{V}}\mathrm{d}^2\vec{r}\,\frac{(\vec{n}_{\vec{r}'}\cdot\vec{e}_z)(\vec{n}_{\vec{r}}\cdot\vec{e}_z)}{|\vec{r}-\vec{r}'|} \\ &= \frac{\mu_0 M_s^2}{2\pi}\int_{\Omega\cap\mathcal{R}_\mathrm{c}}\mathrm{d}^3\vec{r}'\int_\mathcal{V}\mathrm{d}^3\vec{r}\,\Delta_{\vec{r}}\left(\frac{1}{|\vec{r}-\vec{r}'|}\right) = -2\mu_0 M_s^2\int_{\Omega\cap\mathcal{R}_\mathrm{c}}\mathrm{d}^3\vec{r}'\int_\mathcal{V}\mathrm{d}^3\vec{r}\,\delta(\vec{r}-\vec{r}') \\ &= -2\mu_0 M_s^2\pi R^2 h, \end{aligned} \tag{3.40}$$

in agreement with Ref. 10.

Self-energy of the cylinder E_c For the self-energy of the cylinder, the same arguments as for E_f and $E_{\mathrm{c}\leftrightarrow\mathrm{f}}$ apply:

$$\begin{aligned}
E_\mathrm{c} &= 4g(\omega\cap\mathcal{R}_\mathrm{c},\omega\cap\mathcal{R}_\mathrm{c}) = \frac{\mu_0 M_s^2}{2\pi}\int_{\partial(\Omega\cap\mathcal{R}_\mathrm{c})}\mathrm{d}^2\vec{r}'\int_{\partial(\Omega\cap\mathcal{R}_\mathrm{c})}\mathrm{d}^2\vec{r}\,\frac{(\vec{n}_{\vec{r}'}\cdot\vec{e}_z)(\vec{n}_{\vec{r}}\cdot\vec{e}_z)}{|\vec{r}-\vec{r}'|}\\
&= \frac{\mu_0 M_s^2}{2\pi}\left(4\pi\int_{\Omega\cap\mathcal{R}_\mathrm{c}}\mathrm{d}^3\vec{r}'\int_{\Omega\cap\mathcal{R}_\mathrm{c}}\mathrm{d}^3\vec{r}\,\delta(\vec{r}-\vec{r}')\right.\\
&\qquad\left.-\int_{\partial(\Omega\cap\mathcal{R}_\mathrm{c})}\mathrm{d}^2\vec{r}'\int_{\partial(\Omega\cap\mathcal{R}_\mathrm{c})}\mathrm{d}^2\vec{r}\,\frac{(\vec{n}_{\vec{r}'}\cdot\vec{e}_x)(\vec{n}_{\vec{r}}\cdot\vec{e}_x)+(\vec{n}_{\vec{r}'}\cdot\vec{e}_y)(\vec{n}_{\vec{r}}\cdot\vec{e}_y)}{|\vec{r}-\vec{r}'|}\right)\\
&= \frac{\mu_0 M_s^2}{2\pi}\left(4\pi^2R^2h-\int_{\partial(\Omega\cap\mathcal{R}_\mathrm{c})}\mathrm{d}^2\vec{r}'\int_{\partial(\Omega\cap\mathcal{R}_\mathrm{c})}\mathrm{d}^2\vec{r}\,\frac{(\vec{n}_{\vec{r}'}\cdot\vec{e}_x)(\vec{n}_{\vec{r}}\cdot\vec{e}_x)+(\vec{n}_{\vec{r}'}\cdot\vec{e}_y)(\vec{n}_{\vec{r}}\cdot\vec{e}_y)}{|\vec{r}-\vec{r}'|}\right).
\end{aligned}\tag{3.41}$$

The second term can be simplified as follows:

$$\begin{aligned}
&\frac{\mu_0 M_s^2}{2\pi}\int_{\partial(\Omega\cap\mathcal{R}_\mathrm{c})}\mathrm{d}^2\vec{r}'\int_{\partial(\Omega\cap\mathcal{R}_\mathrm{c})}\mathrm{d}^2\vec{r}\,\frac{(\vec{n}_{\vec{r}'}\cdot\vec{e}_x)(\vec{n}_{\vec{r}}\cdot\vec{e}_x)+(\vec{n}_{\vec{r}'}\cdot\vec{e}_y)(\vec{n}_{\vec{r}}\cdot\vec{e}_y)}{|\vec{r}-\vec{r}'|}\\
&=\frac{\mu_0 M_s^2}{2\pi}\int_{r_x^2+r_y^2=R^2,\,0\le z\le h}\mathrm{d}^2\vec{r}'\int_{r_x^2+r_y^2=R^2,\,0\le z\le h}\mathrm{d}^2\vec{r}\,\frac{(\vec{n}_{\vec{r}'}\cdot\vec{e}_x)(\vec{n}_{\vec{r}}\cdot\vec{e}_x)+(\vec{n}_{\vec{r}'}\cdot\vec{e}_y)(\vec{n}_{\vec{r}}\cdot\vec{e}_y)}{|\vec{r}-\vec{r}'|}.
\end{aligned}\tag{3.42}$$

Using polar coordinates, $\vec{n}_{\vec{r}}=\cos(\varphi)\vec{e}_x+\sin(\varphi)\vec{e}_y$ and $\vec{n}_{\vec{r}'}=\cos(\varphi')\vec{e}_x+\sin(\varphi')\vec{e}_y$, the result is:

$$\begin{aligned}
&\frac{\mu_0 M_s^2}{2\pi}\int_{r_x^2+r_y^2=R^2,\,0\le z\le h}\mathrm{d}^2\vec{r}'\int_{r_x^2+r_y^2=R^2,\,0\le z\le h}\mathrm{d}^2\vec{r}\,\frac{(\vec{n}_{\vec{r}'}\cdot\vec{e}_x)(\vec{n}_{\vec{r}}\cdot\vec{e}_x)+(\vec{n}_{\vec{r}'}\cdot\vec{e}_y)(\vec{n}_{\vec{r}}\cdot\vec{e}_y)}{|\vec{r}-\vec{r}'|}\\
&=\frac{\mu_0 M_s^2R^2}{2\pi}\int_0^{2\pi}\mathrm{d}\varphi\int_0^{2\pi}\mathrm{d}\varphi'\int_0^h\mathrm{d}z\int_0^h\mathrm{d}z'\,\frac{\cos(\varphi-\varphi')}{\sqrt{(z-z')^2+2R^2(1-\cos(\varphi-\varphi'))}}\\
&=\frac{\mu_0 M_s^2R^2}{2\pi}\int_0^{2\pi}\mathrm{d}\varphi\int_0^{2\pi}\mathrm{d}\varphi' 2\cos(\varphi-\varphi')\left(-\sqrt{h^2-2R^2\cos(\varphi-\varphi')+2R^2}\right.\\
&\qquad\left.+h\tanh^{-1}\left(\frac{h}{\sqrt{h^2-2R^2\cos(\varphi-\varphi')+2R^2}}\right)+\sqrt{2R^2(1-\cos(\varphi-\varphi'))}\right)\\
&=\frac{2}{3}\mu_0 M_s^2\left(\left(h^3+4hR^2\right)\mathrm{K}\left(-\frac{4R^2}{h^2}\right)-\left(h^3-4hR^2\right)\mathrm{E}\left(-\frac{4R^2}{h^2}\right)-8R^3\right)
\end{aligned}\tag{3.43}$$

where $\mathrm{K}(x)$ is the complete elliptic integral of the first kind, and $\mathrm{E}(x)$ is the complete elliptic integral of the second kind. Thus, the self-energy of the cylinder is:

$$E_\mathrm{c}=\frac{2}{3}\mu_0 M_s^2\left(R^2(3h\pi+8R)-\left(h^3+4hR^2\right)\mathrm{K}\left(-\frac{4R^2}{h^2}\right)+\left(h^3-4hR^2\right)\mathrm{E}\left(-\frac{4R^2}{h^2}\right)\right).\tag{3.44}$$

This corresponds to the result in Ref. 10 and Ref. 11, however the full derivation was not provided.

Interaction of cylinder in the considered unit cell with all the other cylinders in the cylinder lattice $E_{c\leftrightarrow c}$ To calculate the interaction of a single cylinder with the cylinder lattice $E_{\mathrm{c}\leftrightarrow\mathrm{c}}$, we will first decompose this term into individual cylinder-cylinder interactions. Then, we will calculate the interaction of two cylinders $E_{s,\mathrm{c}\leftrightarrow\mathrm{c}}$, and then calculate the interaction of a single cylinder with the cylinder lattice $E_{\mathrm{c}\leftrightarrow\mathrm{c}}$ for square and hexagonal lattices.

$E_{\mathrm{c}\leftrightarrow\mathrm{c}}$ can be rewritten as individual cylinder-cylinder interactions:

$$\begin{aligned}
E_{\mathrm{c}\leftrightarrow\mathrm{c}} &= 4g(\omega\cap\mathcal{R}_{\mathrm{c}},(\mathbb{R}^2\setminus\omega)\cap\mathcal{R}_{\mathrm{c}}) = 4\frac{\mu_0 M_s^2}{8\pi}\int_{\omega\cap\mathcal{R}_{\mathrm{c}}}\mathrm{d}^2\vec{r}'\int_{(\mathbb{R}^2\setminus\omega)\cap\mathcal{R}_{\mathrm{c}})}\mathrm{d}^2\vec{r}\,2\left(\frac{1}{|\vec{r}-\vec{r}'|}-\frac{1}{|\vec{r}-\vec{r}'+\vec{e}_z h|}\right)\\
&= \frac{\mu_0 M_s^2}{\pi}\sum_{\substack{(i,j)\in\mathbb{Z}^2,\\(i,j)\neq(0,0)}}\int_{|\vec{r}'|\le R}\mathrm{d}^2\vec{r}'\int_{|\vec{r}-(i\vec{v}_1+j\vec{v}_2)|\le R}\mathrm{d}^2\vec{r}\left(\frac{1}{|\vec{r}-\vec{r}'|}-\frac{1}{|\vec{r}-\vec{r}'+\vec{e}_z h|}\right)\\
&= \sum_{\substack{(i,j)\in\mathbb{Z}^2,\\(i,j)\neq(0,0)}}E_{\mathrm{s,c}\leftrightarrow\mathrm{c}}(i\vec{v}_1+j\vec{v}_2).
\end{aligned}\tag{3.45}$$

Here, $E_{\mathrm{s,c}\leftrightarrow\mathrm{c}}(\vec{R})$ represents the interaction between two cylinders, where $\vec{R}$ is the vector pointing from the center of the first cylinder to the center of the second cylinder and can be written as:

$$E_{\mathrm{s,c}\leftrightarrow\mathrm{c}}(\vec{R}) = \frac{\mu_0 M_s^2}{\pi}\int_{|\vec{r}'|\le R}\mathrm{d}^2\vec{r}'\int_{|\vec{r}-\vec{R}|\le R}\mathrm{d}^2\vec{r}\left(\frac{1}{\sqrt{(x-x')^2+(y-y')^2}}-\frac{1}{\sqrt{(x-x')^2+(y-y')^2+h^2}}\right),\tag{3.46}$$

and rewritten in polar coordinates, it follows:

$$\begin{aligned}
E_{\mathrm{s,c}\leftrightarrow\mathrm{c}}(\vec{R}) = \mu_0 M_s^2\int_0^{2\pi}\mathrm{d}\varphi_1\int_0^{2\pi}\mathrm{d}\varphi_2\int_0^R\mathrm{d}r_1\int_0^R\mathrm{d}r_2\, r_1 r_2\\
\mathcal{I}(r_1\cos(\varphi_1)-r_2\cos(\varphi_2),r_1\sin(\varphi_1)-r_2\sin(\varphi_2),0,R_x,R_y,0)\\
-\mathcal{I}(r_1\cos(\varphi_1)-r_2\cos(\varphi_2),r_1\sin(\varphi_1)-r_2\sin(\varphi_2),0,R_x,R_y,h),
\end{aligned}\tag{3.47}$$

with

$$\mathcal{I}(r_x,r_y,r_z,R_x,R_y,R_z) = \frac{1}{\pi\sqrt{(r_x-R_x)^2+(r_y-R_y)^2+(r_z-R_z)^2}}.\tag{3.48}$$

To calculate the integral, a multipole expansion of $\mathcal{I}$ is performed up to order N:

$$\begin{aligned}
\mathcal{I}_{\mathcal{T}}(r_x,r_y,r_z,R_x,R_y,R_z) &= \sum_{n=0}^{N}\mathcal{I}_{\mathcal{T}}^{(n)}(r_x,r_y,r_z,R_x,R_y,R_z)\\
\mathcal{I}_{\mathcal{T}}^{(n)}(r_x,r_y,r_z,R_x,R_y,R_z) &= \sum_{|\alpha|=n}\frac{r^\alpha}{\alpha!}\,\partial^\alpha\mathcal{I}(r_x,r_y,r_z,R_x,R_y,R_z)\big|_{r_x=0,r_y=0,r_z=0},
\end{aligned}\tag{3.49}$$

where multi-index notation $\alpha=(\alpha_1,\alpha_2,\alpha_3)$ is employed, with $|\alpha|=\sum_i\alpha_i$, $\alpha!=\prod_i\alpha_i!$, $r^\alpha=\prod_i r_i^{\alpha_i}$, and $\partial^\alpha=\prod_i\partial_{\alpha_i}$, where $(r_x,r_y,r_z)=(r_1,r_2,r_3)$. With this expansion, Equation 3.47 can be calculated with the following approximation:

$$\begin{aligned}
E_{\mathrm{s,c}\leftrightarrow\mathrm{c}}(\vec{R}) &= \mu_0 M_s^2\sum_{n=0}^{N}E_{\mathrm{s,c}\leftrightarrow\mathrm{c}}^{(n)}(\vec{R})\\
E_{\mathrm{s,c}\leftrightarrow\mathrm{c}}^{(n)}(\vec{R}) &= \int_0^{2\pi}\mathrm{d}\varphi_1\int_0^{2\pi}\mathrm{d}\varphi_2\int_0^R\mathrm{d}r_1\int_0^R\mathrm{d}r_2\, r_1 r_2\,\mathcal{I}^{(n)}(r_1\cos(\varphi_1)-r_2\cos(\varphi_2),r_1\sin(\varphi_1))\\
&\quad -r_2\sin(\varphi_2),0,R_x,R_y,0)-\mathcal{I}^{(n)}(r_1\cos(\varphi_1)-r_2\cos(\varphi_2),r_1\sin(\varphi_1))\\
&\quad -r_2\sin(\varphi_2),0,R_x,R_y,h).
\end{aligned}\tag{3.50}$$

The solutions for $E^{(n)}_{\mathrm{s,c\leftrightarrow c}}(\vec{X})$ with $L = |\vec{R}| = \sqrt{R_x^2 + R_y^2}$ are:

$$
\begin{aligned}
E^{(0)}_{\mathrm{s,c\leftrightarrow c}}(\vec{R}) &= \pi R^4 \left(\frac{1}{L} - \frac{1}{\sqrt{h^2 + L^2}} \right) \\
E^{(2)}_{\mathrm{s,c\leftrightarrow c}}(\vec{R}) &= \frac{1}{4}\pi R^6 \left(\frac{2h^2 - L^2}{(h^2 + L^2)^{5/2}} + \frac{1}{L^3} \right) \\
E^{(4)}_{\mathrm{s,c\leftrightarrow c}}(\vec{R}) &= \frac{5}{64}\pi R^8 \left(\frac{-8h^4 + 24h^2L^2 - 3L^4}{(h^2 + L^2)^{9/2}} + \frac{3}{L^5} \right) \\
E^{(6)}_{\mathrm{s,c\leftrightarrow c}}(\vec{R}) &= \frac{35}{512}\pi R^{10} \left(\frac{16h^6 - 120h^4L^2 + 90h^2L^4 - 5L^6}{(h^2 + L^2)^{13/2}} + \frac{5}{L^7} \right) \\
E^{(8)}_{\mathrm{s,c\leftrightarrow c}}(\vec{R}) &= \frac{147\pi}{8192} R^{12} \left(\frac{-128h^8 + 1792h^6L^2 - 3360h^4L^4 + 1120h^2L^6 - 35L^8}{(h^2 + L^2)^{17/2}} + \frac{35}{L^9} \right) \\
E^{(10)}_{\mathrm{s,c\leftrightarrow c}}(\vec{R}) &= \frac{693\pi}{32768} R^{14} \left(\frac{256h^{10} - 5760h^8L^2 + 20160h^6L^4 - 16800h^4L^6 + 3150h^2L^8 - 63L^{10}}{(h^2 + L^2)^{21/2}} + \frac{63}{L^{11}} \right) \\
E^{(1)}_{\mathrm{s,c\leftrightarrow c}}(\vec{R}) &= E^{(3)}_{\mathrm{s,c\leftrightarrow c}}(\vec{R}) = E^{(5)}_{\mathrm{s,c\leftrightarrow c}}(\vec{R}) = E^{(7)}_{\mathrm{s,c\leftrightarrow c}}(\vec{R}) = E^{(9)}_{\mathrm{s,c\leftrightarrow c}}(\vec{R}) = E^{(11)}_{\mathrm{s,c\leftrightarrow c}}(\vec{R}) = 0.
\end{aligned}
\tag{3.51}
$$

The dependence solely on L rather than on R_x and R_y individually arises from the rotational symmetry of the two-cylinder system. Thus, it also holds that:

$$E_{\mathrm{s,c\leftrightarrow c}}(\vec{R}) = E_{\mathrm{s,c\leftrightarrow c}}(|\vec{R}|) \tag{3.52}$$

with $E_{\mathrm{s,c\leftrightarrow c}}(\vec{R})$ calculated, the interaction of the cylinder in the considered unit cell with all other cylinders in the cylinder lattice, $E_{\mathrm{c\leftrightarrow c}}$, can now be calculated, first for the **square lattice** and then for the **hexagonal lattice**.

Square lattice For the square lattice, it holds that:

$$E_{\mathrm{c\leftrightarrow c}} = \sum_{\substack{(i,j)\in\mathbb{Z}^2,\\ (i,j)\neq(0,0)}} E_{\mathrm{s,c\leftrightarrow c}}(|i\vec{v}_1 + j\vec{v}_2|) = \sum_{\substack{(i,j)\in\mathbb{Z}^2,\\ (i,j)\neq(0,0)}} E_{\mathrm{s,c\leftrightarrow c}}(P\sqrt{i^2 + j^2}). \tag{3.53}$$

The cornerstone for the subsequent calculations is the Euler-Maclaurin formula[12]:

$$\sum_{i=p}^{q} f(i) = \int_p^q f(i)\,\mathrm{d}i + \frac{f(p) + f(q)}{2} + \sum_{\nu=1}^{n} \frac{B_{2\nu}}{(2\nu)!} \left(f^{(2\nu-1)}(q) - f^{(2\nu-1)}(p) \right) + R_n \tag{3.54}$$

where B_n are the Bernoulli numbers, $f^{(n)}(q) = \frac{\mathrm{d}^n f(q)}{\mathrm{d}q^n}$, and R_n is the remainder term (for $f^{(2n)}$ being monotonically increasing):

$$|R_n(p,q)| \leq \frac{1}{2} \left(1 - \frac{2}{2^{2n}} \right) \frac{|B_{2n}|}{(2n)!} |f^{(2n)}(q) - f^{(2n)}(p)|. \tag{3.55}$$

Thus, it makes sense to explicitly calculate the first terms of the sum and to apply the Euler-Maclaurin formula only for $p > 1$ in order to minimize $|R_n(p,q)|$. For example, for $\sum_{i=0}^{\infty} f(i) = f(0) + f(1) + \sum_{i=2}^{\infty} f(i)$, it would be advantageous to apply the Euler-Maclaurin formula only

to $\sum_{i=2}^{\infty} f(i)$.

$E_{\mathrm{c}\leftrightarrow\mathrm{c}}$ will now be split into the following components, which describe the interaction in different regions:

$$
\begin{aligned}
E_{\mathrm{c}\leftrightarrow\mathrm{c}} &= 4E_{\mathrm{s,c}\leftrightarrow\mathrm{c}}(P) + 4E_{\mathrm{s,c}\leftrightarrow\mathrm{c}}(\sqrt{2}P) + 4E_{\mathrm{c}\leftrightarrow\mathrm{c},(j=0,i\geq 2)} + 8E_{\mathrm{c}\leftrightarrow\mathrm{c},(j=1,i\geq 2)} + 4E_{\mathrm{c}\leftrightarrow\mathrm{c},(j\geq 2,i\geq 2)} \\
E_{\mathrm{c}\leftrightarrow\mathrm{c},(j=0,i\geq 2)} &= \sum_{i=2}^{\infty} E_{\mathrm{s,c}\leftrightarrow\mathrm{c}}(Pi) \\
E_{\mathrm{c}\leftrightarrow\mathrm{c},(j=1,i\geq 2)} &= \sum_{i=2}^{\infty} E_{\mathrm{s,c}\leftrightarrow\mathrm{c}}(P\sqrt{i^2+1}) \\
E_{\mathrm{c}\leftrightarrow\mathrm{c},(j\geq 2,i\geq 2)} &= \sum_{j=2}^{\infty}\sum_{i=2}^{\infty} E_{\mathrm{s,c}\leftrightarrow\mathrm{c}}(P\sqrt{i^2+j^2})
\end{aligned}
\tag{3.56}
$$

We have highlighted each region in different color to ease the follow up of Figure S4. The begin is at $p = 2$ for the two-dimensional and one-dimensional sums, as this results in a smaller remainder term, as explained above.

The Euler-Maclaurin formula is now applied as follows to obtain an analytical expression for $E_{\mathrm{c}\leftrightarrow\mathrm{c}}$ in good approximation for the series. For this, the auxiliary functions are introduced, to which the Euler-Maclaurin formula is applied:

$$
\begin{aligned}
H_1(s_i,j) = \sum_{i=s_i}^{\infty} E_{\mathrm{s,c}\leftrightarrow\mathrm{c}}(P\sqrt{i^2+j^2}) &= \int_{s_i}^{\infty} E_{\mathrm{s,c}\leftrightarrow\mathrm{c}}(P\sqrt{i^2+j^2})\mathrm{d}i + \frac{E_{\mathrm{s,c}\leftrightarrow\mathrm{c}}(P\sqrt{s_i^2+j^2})}{2} \\
&\quad - \sum_{\nu=1}^{n=5} \frac{B_{2\nu}}{(2\nu)!} \left.\frac{\mathrm{d}^{2\nu-1}E_{\mathrm{s,c}\leftrightarrow\mathrm{c}}(P\sqrt{i^2+j^2})}{\mathrm{d}i^{2\nu-1}}\right|_{i=s_i} \\
H_2(s_i,s_j) = \sum_{j=s_j}^{\infty} H_1(s_i,j) &= \int_{s_j}^{\infty} H_1(s_i,j)\mathrm{d}j + \frac{H_1(s_i,s_j)}{2} - \sum_{\nu=1}^{n=5} \frac{B_{2\nu}}{(2\nu)!} \left.\frac{\mathrm{d}^{2\nu-1}H_1(s_i,j)}{\mathrm{d}j^{2\nu-1}}\right|_{j=s_j} \\
H_3(s_i) = \sum_{i=s_i}^{\infty} E_{\mathrm{s,c}\leftrightarrow\mathrm{c}}(Pi) &= \int_{s_i}^{\infty} E_{\mathrm{s,c}\leftrightarrow\mathrm{c}}(Pi)\mathrm{d}i + \frac{E_{\mathrm{s,c}\leftrightarrow\mathrm{c}}(Ps_i)}{2} - \sum_{\nu=1}^{n=5} \frac{B_{2\nu}}{(2\nu)!} \left.\frac{\mathrm{d}^{2\nu-1}E_{\mathrm{s,c}\leftrightarrow\mathrm{c}}(Pi)}{\mathrm{d}i^{2\nu-1}}\right|_{i=s_i}.
\end{aligned}
\tag{3.57}
$$

This results now in:

$$
E_{\mathrm{c}\leftrightarrow\mathrm{c},(j=0,i\geq 2)} = H_3(2) \quad E_{\mathrm{c}\leftrightarrow\mathrm{c},(j=1,i\geq 2)} = H_1(2,1) \quad E_{\mathrm{c}\leftrightarrow\mathrm{c},(j\geq 2,i\geq 2)} = H_2(2,2) \tag{3.58}
$$

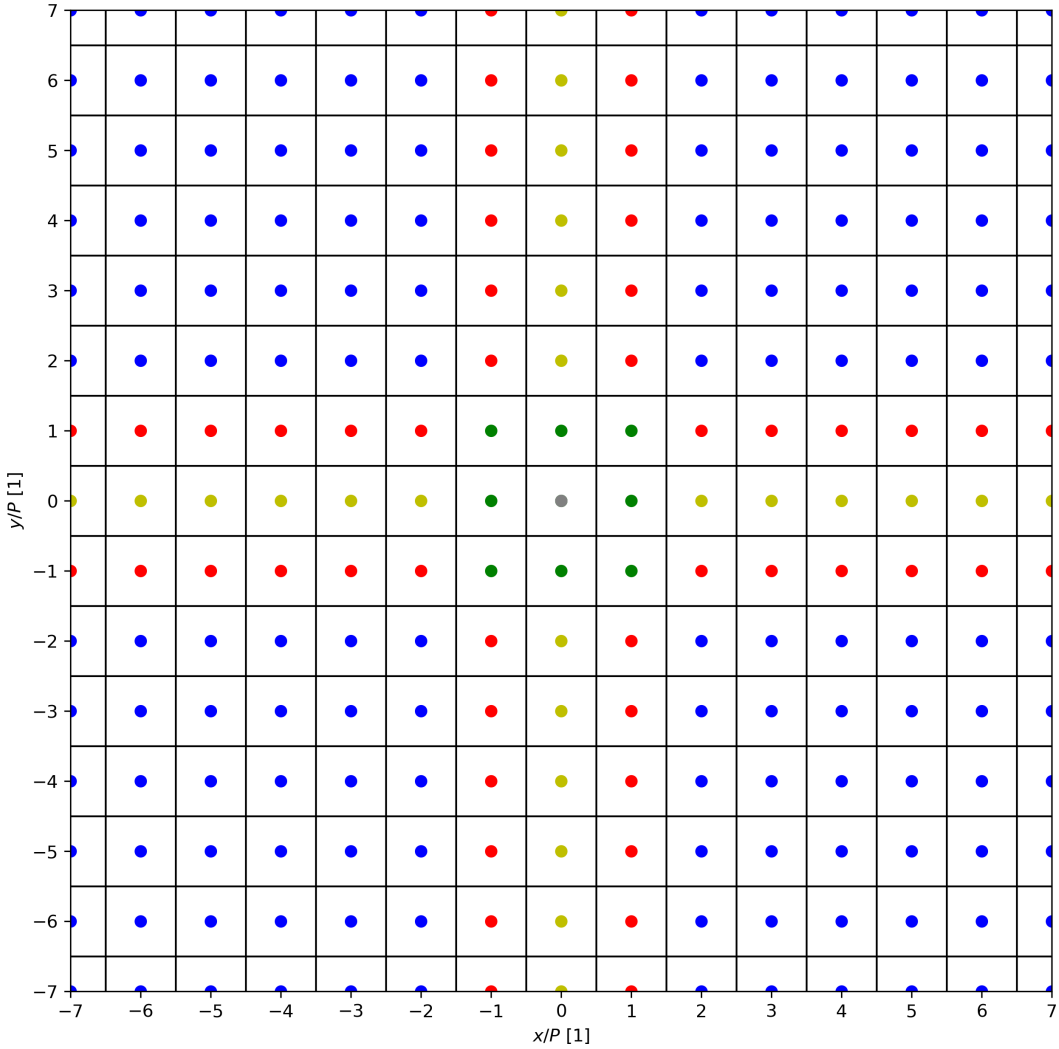

Figure S 4: Decomposition of the square lattice into different regions for the application of the Euler-Maclaurin formula. The colours correspond to each region defined in Equation 3.56

The analytical terms for $E_{\mathrm{c}\leftrightarrow\mathrm{c}}$ follow from Equation 3.56, Equation 3.57, Equation 3.58. The terms resulting from the analytical integration are not explicitly stated here; for $E^{(1)}_{\mathrm{s,c}\leftrightarrow\mathrm{c}}(\vec{R})$, there are 70 terms, while for $E^{(11)}_{\mathrm{s,c}\leftrightarrow\mathrm{c}}(\vec{R})$, there are over 1000 terms. Nevertheless, compact analytical formulae for $E_{\mathrm{c}\leftrightarrow\mathrm{c}}$ can be found for various limits, which will be derived and explicitly stated later. Beyond these limits, a numerical minimization will need to be performed; the relevant results will also be provided later.

Hexagonal lattice For the hexagonal lattice, the following applies:

$$E_{\mathrm{c}\leftrightarrow\mathrm{c}} = \sum_{\substack{(i,j)\in\mathbb{Z}^2,\\(i,j)\neq(0,0)}} E_{\mathrm{s,c}\leftrightarrow\mathrm{c}}(|i\vec{v}_1 + j\vec{v}_2|) = \sum_{\substack{(i,j)\in\mathbb{Z}^2,\\(i,j)\neq(0,0)}} E_{\mathrm{s,c}\leftrightarrow\mathrm{c}}(P\sqrt{i^2+j^2-ij}) \tag{3.59}$$

$E_{\mathrm{c}\leftrightarrow\mathrm{c}}$ is now similarly split, although the splitting is slightly more complex:

$$
\begin{aligned}
E_{\mathrm{c}\leftrightarrow\mathrm{c}} &= 6E_{\mathrm{s,c}\leftrightarrow\mathrm{c}}(P) + 6E_{\mathrm{s,c}\leftrightarrow\mathrm{c}}(\sqrt{3}P) + 4E_{\mathrm{c}\leftrightarrow\mathrm{c},(j=0,i\geq 2)} + 8E_{\mathrm{c}\leftrightarrow\mathrm{c},(j=1,i\geq 3)} \\
&\quad + 2E_{\mathrm{c}\leftrightarrow\mathrm{c},(j\geq 2,i\geq 2)} + 2E_{\mathrm{c}\leftrightarrow\mathrm{c},(j\geq 2,i\leq -2)} \\
E_{\mathrm{c}\leftrightarrow\mathrm{c},(j=0,i\geq 2)} &= \sum_{i=2}^{\infty} E_{\mathrm{s,c}\leftrightarrow\mathrm{c}}(Pi) \quad E_{\mathrm{c}\leftrightarrow\mathrm{c},(j=1,i\geq 3)} = \sum_{i=3}^{\infty} E_{\mathrm{s,c}\leftrightarrow\mathrm{c}}(P\sqrt{i^2+1-i}) \\
E_{\mathrm{c}\leftrightarrow\mathrm{c},(j\geq 2,i\geq 2)} &= \sum_{j=2}^{\infty}\sum_{i=2}^{\infty} E_{\mathrm{s,c}\leftrightarrow\mathrm{c}}(P\sqrt{i^2+j^2-ij}) \quad E_{\mathrm{c}\leftrightarrow\mathrm{c},(j\geq 2,i\leq -2)} = \sum_{j=2}^{\infty}\sum_{i=-\infty}^{-2} E_{\mathrm{s,c}\leftrightarrow\mathrm{c}}(P\sqrt{i^2+j^2-ij}).
\end{aligned}
\tag{3.60}
$$

We have again highlighted each region in different color to ease the follow up of Figure S5. With the auxiliary functions that apply the Euler-Maclaurin formula, it follows that:

$$
\begin{aligned}
H_1(s_i,j) = \sum_{i=s_i}^{\infty} E_{\mathrm{s,c}\leftrightarrow\mathrm{c}}(P\sqrt{i^2+j^2-ij}) &= \int_{s_i}^{\infty} E_{\mathrm{s,c}\leftrightarrow\mathrm{c}}(P\sqrt{i^2+j^2-ij})\mathrm{d}i + \frac{E_{\mathrm{s,c}\leftrightarrow\mathrm{c}}(P\sqrt{s_i^2+j^2-s_ij})}{2} \\
&\quad - \sum_{\nu=1}^{n=5} \frac{B_{2\nu}}{(2\nu)!} \left.\frac{\mathrm{d}^{2\nu-1}E_{\mathrm{s,c}\leftrightarrow\mathrm{c}}(P\sqrt{i^2+j^2-ij})}{\mathrm{d}i^{2\nu-1}}\right|_{i=s_i} \\
H_2(s_i,s_j) = \sum_{j=s_j}^{\infty} H_1(s_i,j) &= \int_{s_j}^{\infty} H_1(s_i,j)\mathrm{d}j + \frac{H_1(s_i,s_j)}{2} - \sum_{\nu=1}^{n=5} \frac{B_{2\nu}}{(2\nu)!} \left.\frac{\mathrm{d}^{2\nu-1}H_1(s_i,j)}{\mathrm{d}j^{2\nu-1}}\right|_{j=s_j} \\
H_3(s_i,j) = \sum_{i=-\infty}^{s_i} E_{\mathrm{s,c}\leftrightarrow\mathrm{c}}(P\sqrt{i^2+j^2-ij}) &= \int_{-\infty}^{s_i} E_{\mathrm{s,c}\leftrightarrow\mathrm{c}}(P\sqrt{i^2+j^2-ij})\mathrm{d}i + \frac{E_{\mathrm{s,c}\leftrightarrow\mathrm{c}}(P\sqrt{s_i^2+j^2-s_ij})}{2} \\
&\quad + \sum_{\nu=1}^{n=5} \frac{B_{2\nu}}{(2\nu)!} \left.\frac{\mathrm{d}^{2\nu-1}E_{\mathrm{s,c}\leftrightarrow\mathrm{c}}(P\sqrt{i^2+j^2-ij})}{\mathrm{d}i^{2\nu-1}}\right|_{i=s_i} \\
H_4(s_i,s_j) = \sum_{j=s_j}^{\infty} H_1(s_i,j) &= \int_{s_j}^{\infty} H_1(s_i,j)\mathrm{d}j + \frac{H_1(s_i,s_j)}{2} - \sum_{\nu=1}^{n=5} \frac{B_{2\nu}}{(2\nu)!} \left.\frac{\mathrm{d}^{2\nu-1}H_3(s_i,j)}{\mathrm{d}j^{2\nu-1}}\right|_{j=s_j} \\
H_5(s_i) = \sum_{i=s_i}^{\infty} E_{\mathrm{s,c}\leftrightarrow\mathrm{c}}(Pi) &= \int_{s_i}^{\infty} E_{\mathrm{s,c}\leftrightarrow\mathrm{c}}(Pi)\mathrm{d}i + \frac{E_{\mathrm{s,c}\leftrightarrow\mathrm{c}}(Ps_i)}{2} - \sum_{\nu=1}^{n=5} \frac{B_{2\nu}}{(2\nu)!} \left.\frac{\mathrm{d}^{2\nu-1}E_{\mathrm{s,c}\leftrightarrow\mathrm{c}}(Pi)}{\mathrm{d}i^{2\nu-1}}\right|_{i=s_i}.
\end{aligned}
\tag{3.61}
$$

And the various contributions to $E_{\mathrm{c}\leftrightarrow\mathrm{c}}$ are thus:

$$
\begin{aligned}
E_{\mathrm{c}\leftrightarrow\mathrm{c},(j=0,i\geq 2)} &= H_5(2) \quad E_{\mathrm{c}\leftrightarrow\mathrm{c},(j=1,i\geq 3)} = H_1(3,1) \\
E_{\mathrm{c}\leftrightarrow\mathrm{c},(j\geq 2,i\geq 2)} &= H_2(2,2) \quad E_{\mathrm{c}\leftrightarrow\mathrm{c},(j\geq 2,i\leq -2)} = H_4(-2,2)
\end{aligned}
\tag{3.62}
$$

For the calculation of $E_{\mathrm{c}\leftrightarrow\mathrm{c}}$ for the hexagonal lattice (with Equation 3.60, Equation 3.61, Equation 3.62), only the first four orders of the multipole expansion of $E_{\mathrm{s,c}\leftrightarrow\mathrm{c}}(\vec{R})$ are used, i.e.,

$$
E_{\mathrm{s,c}\leftrightarrow\mathrm{c}}(\vec{R}) = \sum_{n=0}^{4} E^{(n)}_{\mathrm{s,c}\leftrightarrow\mathrm{c}}(\vec{R}).
\tag{3.63}
$$

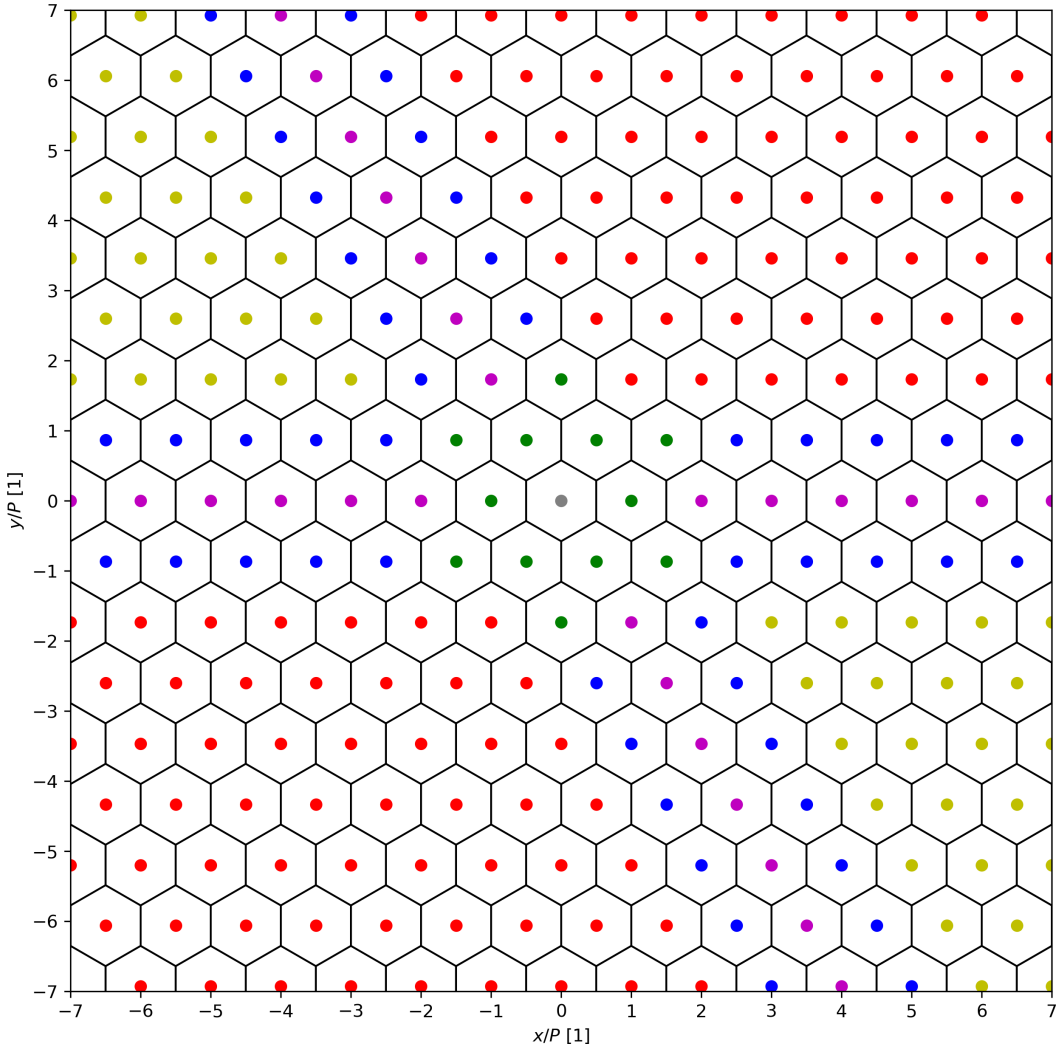

Figure S 5: Decomposition of the hexagonal lattice into different regions for the application of the Euler-Maclaurin formula. The colours correspond to each region defined in Equation 3.60

3.6.5 Deviation from the cylinder lattice approximation for surface charges $E_{\sigma\sigma,\mathrm{nc}}$

The deviation from the cylinder lattice approximation for surface charges can be described as:

$$E_{\sigma\sigma,\mathrm{nc}} = \frac{\mu_0}{8\pi} \int_{\partial\Omega} \mathrm{d}^2\vec{r}' \int_{\partial\mathcal{V}} \mathrm{d}^2\vec{r} \frac{\sigma(\vec{r}')\sigma(\vec{r}) - \sigma_{\Delta\to 0}(\vec{r}')\sigma_{\Delta\to 0}(\vec{r})}{|\vec{r}-\vec{r}'|} \tag{3.64}$$

Since $\sigma(\vec{r}')\sigma(\vec{r}) - \sigma_{\Delta\to 0}(\vec{r}')\sigma_{\Delta\to 0}(\vec{r})$ contributes significantly only at the domain walls of the skyrmions, and since the interaction between positions $\vec{r}$ and $\vec{r}'$ decreases with $\frac{1}{|\vec{r}-\vec{r}'|}$, the interaction between skyrmions is not considered here; instead, only the case of an isolated skyrmion is examined. Therefore,

$$E_{\sigma\sigma,\mathrm{nc}} = \frac{\mu_0}{8\pi} \int_{\partial\mathcal{V}} \mathrm{d}^2\vec{r}' \int_{\partial\mathcal{V}} \mathrm{d}^2\vec{r} \frac{\sigma(\vec{r}')\sigma(\vec{r}) - \sigma_{\Delta\to 0}(\vec{r}')\sigma_{\Delta\to 0}(\vec{r})}{|\vec{r}-\vec{r}'|} \tag{3.65}$$

where σ is now given by $\sigma = M_s\vec{n}\cdot\vec{m}_\mathrm{S}$ and not $\sigma = M_s\vec{n}\cdot\vec{m}_\mathrm{L}$. Furthermore, the curvature effects of the domain wall are neglected, assuming $\Delta \ll R$, and it is replaced by a one-dimensional

infinite domain wall:

$$E_{\sigma\sigma,\mathrm{nc}} = \frac{\mu_0 M_s^2}{8\pi} \lim_{L\to\infty} \frac{2\pi R}{L} \int_{-L/2}^{L/2} \mathrm{d}y \int_{-L/2}^{L/2} \mathrm{d}y' \int_{-\infty}^{\infty} \mathrm{d}x \int_{-\infty}^{\infty} \mathrm{d}x' \, 2(\cos(\theta(x))\cos(\theta(x')) - \cos(\theta_{\Delta\to 0}(x))\cos(\theta_{\Delta\to 0}(x'))) \left(\frac{1}{\sqrt{(x-x')^2+(y-y')^2}} - \frac{1}{\sqrt{(x-x')^2+(y-y')^2+h^2}} \right) \tag{3.66}$$

where $\theta(x)$ is as defined in Equation 3.11, but the domain wall is shifted to $x = 0$; that is, $\cos(\theta(x)) = \tanh(x/\Delta)$. The solution of Equation 3.66 is given by Ref. 13:

$$E_{\sigma\sigma,\mathrm{nc}} = -\mu_0 M_s^2 R \pi^2 \Delta^2 \left(4\psi^{(-2)}\left(\frac{h}{\Delta\pi}\right) - \frac{h}{\Delta\pi^2}\left(4\pi \log\left(\Gamma\left(\frac{h}{\Delta\pi}\right)\right) - 2\frac{h}{\Delta}\log\left(\frac{h}{\Delta}\right) + \frac{h}{\Delta}(1+2\log(\pi)) + 2\pi \right) \right), \tag{3.67}$$

where $\psi^{(n)}(t)$ is the polygamma function of order n.

3.6.6 Volume charge interaction $E_{\rho\rho}$

The interaction of the volume charges $E_{\rho\rho}$ is given by:

$$E_{\rho\rho} = \frac{\mu_0}{8\pi} \int_{\Omega} \mathrm{d}^3\vec{r}' \int_{\mathcal{V}} \mathrm{d}^3\vec{r} \frac{\rho(\vec{r}')\rho(\vec{r})}{|\vec{r}-\vec{r}'|}, \tag{3.68}$$

analogous to $E_{\sigma\sigma,\mathrm{nc}}$, ρ contributes significantly only at the domain wall, and two different domain walls from two skyrmions are far apart. Therefore, the approximation is made that only the domain wall of the same skyrmion is considered, *i.e.*,

$$E_{\rho\rho} = \frac{\mu_0}{8\pi} \int_{\mathcal{V}} \mathrm{d}^3\vec{r}' \int_{\mathcal{V}} \mathrm{d}^3\vec{r} \frac{\rho(\vec{r}')\rho(\vec{r})}{|\vec{r}-\vec{r}'|} \tag{3.69}$$

where $\rho = M_s \nabla\cdot\vec{m}_{\mathrm{S}}$ is from the individual skyrmion. Furthermore, curvature effects are negligible because $\Delta \ll R$, thus

$$E_{\rho\rho} = \frac{\mu_0}{8\pi} 2\pi R \lim_{L\to\infty} \frac{1}{L} \int_{-L/2}^{L/2} \mathrm{d}y \int_{-L/2}^{L/2} \mathrm{d}y' \int_0^h \mathrm{d}z \int_0^h \mathrm{d}z' \int_{-\infty}^{\infty} \mathrm{d}x \int_{-\infty}^{\infty} \mathrm{d}x' \frac{\rho(x)\rho(x')}{|\vec{r}-\vec{r}'|} \tag{3.70}$$

where $\rho(x) = -M_s \partial_x \operatorname{sech}(x/\Delta)$. The solution of this integral is given by Ref. 14:

$$E_{\rho\rho} = 4\pi R \Delta h M_s^2 \mu_0 \left(\frac{\pi\Delta\log\left(\frac{\pi}{A^6}\right)}{2h} + \frac{7\pi\Delta\log(2)}{12h} + \frac{2\pi\Delta\psi^{(-2)}\left(\frac{h}{2\Delta\pi}+\frac{1}{2}\right)}{h} - \frac{2\pi\Delta\psi^{(-2)}\left(\frac{h}{2\Delta\pi}+1\right)}{h} - \log\left(\Gamma\left(\frac{h}{2\Delta\pi}+\frac{1}{2}\right)\right) + \log\left(\Gamma\left(\frac{h}{2\Delta\pi}+1\right)\right)\right). \tag{3.71}$$

3.7 Areal energy density ϵ and equilibrium values of the skyrmion lattice

With the calculated energy terms, the skyrmion lattice model can now be completed. In the following, the material parameters of the effective medium model are used, see Equation 3.2.

The areal energy density ϵ of the considered unit cell, ω, is the key quantity analyzed to determine the energetically stable configurations:

$$\begin{aligned}\epsilon = \frac{E_{\mathrm{tot}}}{\mathrm{area}(\omega)} &= \frac{E_d + E_{\mathrm{ex}} + E_{\mathrm{a}} + E_{\mathrm{DMI}} + E_{\mathrm{Z}}}{\mathrm{area}(\omega)} \\ &= \frac{E_{\rho\rho} + E_{\sigma\sigma,\mathrm{nc}} + E_{\sigma\sigma,\mathrm{c}} + E_{\mathrm{ex}} + E_{\mathrm{a}} + E_{\mathrm{DMI}} + E_{\mathrm{Z}}}{\mathrm{area}(\omega)} \\ &= \frac{2\pi R h \sigma_{\mathrm{DW}}(\Delta) + E_{\sigma\sigma,\mathrm{c}}(R,P,h) + E_{\mathrm{Z}}(B_z,R,h)}{\mathrm{area}(\omega(P))},\end{aligned} \tag{3.72}$$

with the domain wall energy density $\sigma_{\mathrm{DW}}(\Delta)$:

$$\sigma_{\mathrm{DW}}(\Delta) = \frac{E_{\rho\rho} + E_{\sigma\sigma,\mathrm{nc}} + E_{\mathrm{ex}} + E_{\mathrm{a}} + E_{\mathrm{DMI}}}{2\pi R h} \tag{3.73}$$

here $\sigma_{\mathrm{DW}}(\Delta)$ no longer depends on R and P.

The equilibrium values for the parameters Δ, R, P are determined through energy minimization:

$$(R_0, P_0, \Delta_0) = \min_{R,P,\Delta} \epsilon(R,P,\Delta) = \min_{R,P,\Delta} \frac{2\pi R h \sigma_{\mathrm{DW}}(\Delta) + E_{\sigma\sigma,\mathrm{c}}(R,P,h) + E_{\mathrm{Z}}(B_z,R,h)}{\mathrm{area}(\omega(P))}. \tag{3.74}$$

This can first be split into a minimization of Δ:

$$\Delta_0 = \min_{\Delta} \sigma_{\mathrm{DW}}(\Delta) \tag{3.75}$$

and afterwards:

$$(R_0, P_0) = \min_{R,P} \epsilon(R,P) = \min_{R,P} \frac{2\pi R h \sigma_{\mathrm{DW}}(\Delta_0(h)) + E_{\sigma\sigma,\mathrm{c}}(R,P,h) + E_{\mathrm{Z}}(B_z,R,h)}{\mathrm{area}(\omega(P))}. \tag{3.76}$$

Since

$$\begin{aligned} E_{\sigma\sigma,\mathrm{c}}(R,P,h) &= h^3 E_{\sigma\sigma,\mathrm{c}}(R \to R/h, P \to P/h, h \to 1) \\ E_{\mathrm{Z}}(B_z,R,h) &= h E_{\mathrm{Z}}(B_z, R \to R/h, h \to 1) \\ \mathrm{area}(\omega(P)) &= h^2 \,\mathrm{area}(\omega(P \to P/h)), \end{aligned} \tag{3.77}$$

Equation 3.76 can be rewritten as:

$$\begin{aligned}(R_0, P_0) = \min_{R,P} \epsilon(R,P) = \min_{R,P} \frac{1}{\mathrm{area}(\omega(P \to P/h))} \Bigg(& 2\pi \frac{R}{h} \frac{\sigma_{\mathrm{DW}}(\Delta_0(h))}{h \mu_0 M_s^2} \\ & + \frac{E_{\sigma\sigma,\mathrm{c}}(R \to R/h, P \to P/h, h \to 1)}{\mu_0 M_s^2} + \frac{1}{h^2} \frac{E_{\mathrm{Z}}(B_z, R \to R/h, h \to 1)}{\mu_0 M_s^2} \Bigg)\end{aligned} \tag{3.78}$$

where each term in the parentheses is now dimensionless, as are the arguments of $E_{\sigma\sigma,\mathrm{c}}$ and E_{Z}.

3.8 Determination of the domain wall width Δ

To determine the domain wall energy density $\sigma(\Delta, h)$, which no longer depends on R, can be written as:

$$\begin{aligned}
\sigma_{\mathrm{DW}}(\Delta, h) &= \frac{E_{\rho\rho} + E_{\sigma\sigma,\mathrm{nc}} + E_{\mathrm{ex}} + E_{\mathrm{a}} + E_{\mathrm{DMI}}}{2\pi R h} = \sigma_{\mathrm{DW},(A,K,D)}(\Delta) + \sigma_{\mathrm{DW},d}(\Delta, h) \\
\sigma_{\mathrm{DW},(A,K,D)}(\Delta) &= \frac{2A}{\Delta} + 2\Delta K - \pi D \\
\sigma_{\mathrm{DW},d}(\Delta, h) &= \frac{M_s^2 \mu_0}{6\pi h} \left(\pi^2 \Delta^2 \log\left(\frac{128\pi^6}{A^{36}}\right) \right. \\
&\quad -12\pi^2\Delta^2 \left(2\psi^{(-2)}\left(\frac{h}{2\Delta\pi}+1\right) - 2\psi^{(-2)}\left(\frac{1}{2}\left(\frac{h}{\Delta\pi}+1\right)\right) + \psi^{(-2)}\left(\frac{h}{\Delta\pi}\right)\right) \\
&\quad -6h^2 \log\left(\frac{h}{\pi\Delta}\right) + 3h(2\pi\Delta + h) \\
&\quad \left. +12\pi\Delta h \left(\log\left(\Gamma\left(\frac{h}{2\Delta\pi}+1\right)\right) - \log\left(\Gamma\left(\frac{1}{2}\left(\frac{h}{\Delta\pi}+1\right)\right)\right) + \log\left(\Gamma\left(\frac{h}{\Delta\pi}\right)\right)\right)\right).
\end{aligned} \tag{3.79}$$

For a fixed height h, the domain wall width Δ_0 is the one that minimizes the domain wall energy density:

$$\Delta_0 = \min_{\Delta} \sigma_{\mathrm{DW}}(\Delta) \Rightarrow \left.\frac{\partial \sigma_{\mathrm{DW}}}{\partial \Delta}(\Delta)\right|_{\Delta=\Delta_0} \stackrel{!}{=} 0 \tag{3.80}$$

Without the magnetostatic energy ($M_s = 0$), using Equation 3.80, one obtains the well-known formula $\Delta_0 = \sqrt{A/K}$ with $\sigma(\Delta_0) = 4\sqrt{AK} - \pi D$.

In the case with the magnetostatic energy $M_s \neq 0$, for the thin-film limit $h \to 0$, $\sigma_{\mathrm{DW},d}(\Delta, h)$ can be expanded as $\sigma_{\mathrm{DW},d}(\Delta, h) = -\mu_0 M_s^2 \Delta$, leading to $\Delta_0 = \sqrt{A/(K - \mu_0 M_s^2)}$ and $\sigma(\Delta_0) = 4\sqrt{A(K - \mu_0 M_s^2)} - \pi D$. Similarly, with the magnetostatic energy for the thick-film limit $h \to \infty$, one finds $\sigma_{\mathrm{DW},d}(\Delta, h) = \mu_0 M_s^2 \Delta$, leading to $\Delta_0 = \sqrt{A/(K + \mu_0 M_s^2)}$ and $\sigma(\Delta_0) = 4\sqrt{A(K + \mu_0 M_s^2)} - \pi D$. These formulae for the thin-film and thick-film limits have been previously suggested in Ref. 13.

Beyond the thin- and thick-film limits, for arbitrary h, Equation 3.80 is minimized numerically. The results using the material parameters in the effective medium model (see Equation 3.2), $\Delta_0(h)$ and $\lambda = \frac{\sigma(\Delta_0(h), h)}{\mu_0 M_s^2}$, are shown in Figure S6. The quantity $\frac{\sigma_{\mathrm{DW}}(\Delta_0(h), h)}{\mu_0 M_s^2} = \lambda$ is referred to as the characteristic dipolar length[15,16].

The numerically determined solution agrees with the thin-film and thick-film limits at both extremes. The solution without the magnetostatic energy, $\Delta = \sqrt{A/K}$, lies between the two limits. The relationship $\sigma_{\mathrm{DW}} = \sigma_{\mathrm{DW}}(\Delta_0(h))$ shown here will be used in the next step for determining R and P.

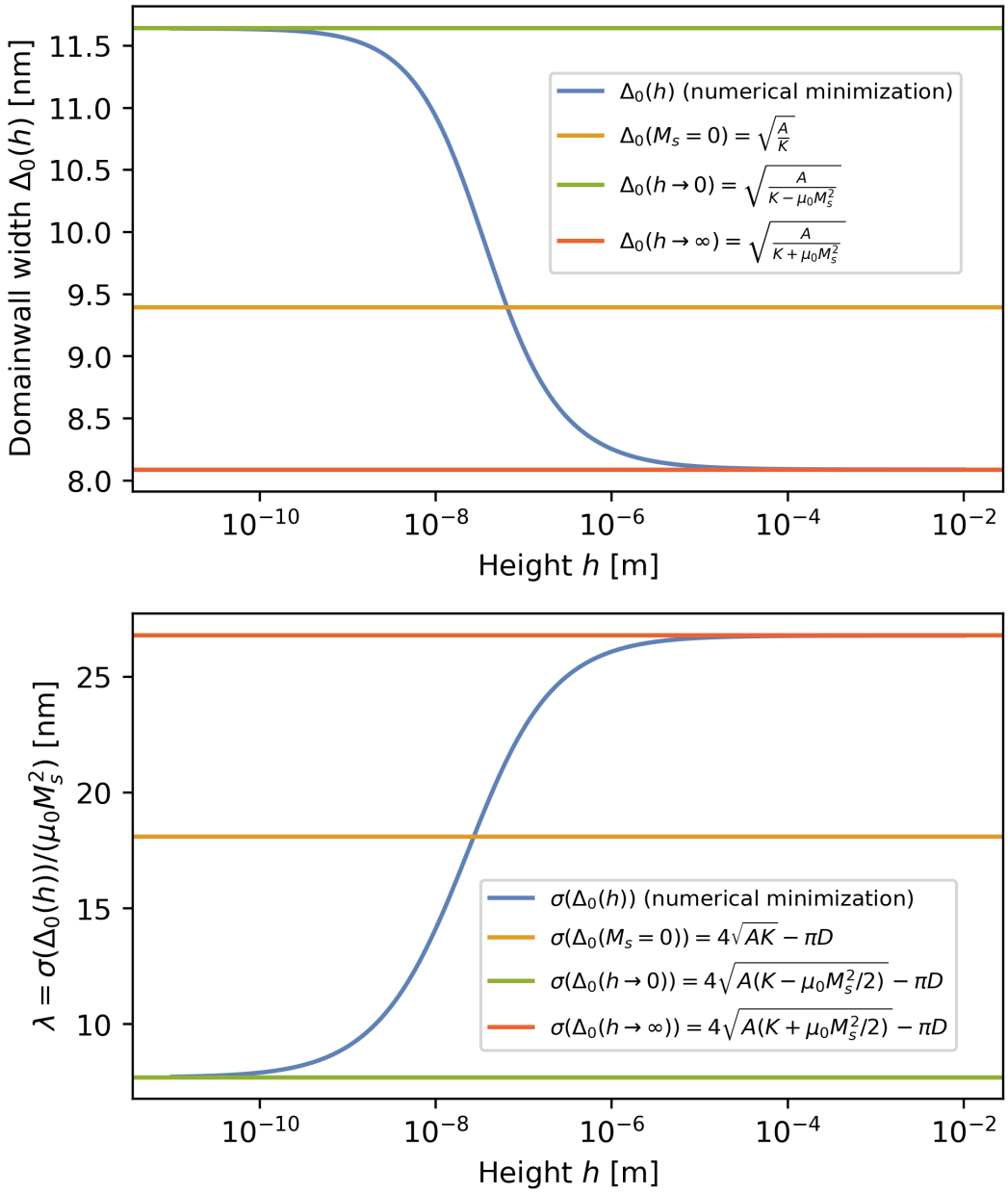

Figure S 6: Domain wall width $\Delta_0(h)$ and the characteristic dipolar length $\frac{\sigma_{\mathrm{DW}}(\Delta_0(h),h)}{\mu_0 M_s^2} = \lambda$ as a function of height h.

3.9 Determination of the equilibrium values of R and P with no external field $B_z = 0$

With the model at hand, we will present now the case for the equilibrium values of the radius R of the skyrmions and the periodicity P of the skyrmion lattice, for the case where no external field is applied, $B_z = 0$. We will first derive the closed analytical formulae, and the, provide numerical results.

3.9.1 Closed analytical formulae

First, the analytical formulae for R and P are derived, which describe the lattice configuration with the lowest energy density ϵ:

$$(R_0, P_0) = \min_{R,P} \frac{2\pi R h \sigma_{\mathrm{DW}} + E_{\sigma\sigma,\mathrm{c}}(R, P, h)}{\mathrm{area}(\omega(P))} \tag{3.81}$$

using the shorthand notation $\sigma_{\mathrm{DW}}(\Delta_0(h), h) = \sigma_{\mathrm{DW}}$.

To obtain the energy minima of Equation 3.81, we first consider again Equation 3.31:

$$E_{\sigma\sigma} = \frac{\mu_0}{8\pi} \int_{\partial\Omega} \mathrm{d}^2\vec{r}' \int_{\partial\mathcal{V}} \mathrm{d}^2\vec{r} \, \frac{\sigma(\vec{r}')\sigma(\vec{r})}{|\vec{r} - \vec{r}'|}. \tag{3.82}$$

From this formula, we can conclude that the energy minimum, to a good approximation, occurs around the values of R and P where the positive and negative surface charges $\sigma = \pm M_s$ are equally distributed (charge neutrality), *i.e.*,

$$\frac{\pi R^2}{\mathrm{area}(\omega(P))} = \frac{1}{2}. \tag{3.83}$$

This gives the following relation for the hexagonal lattice, with $\mathrm{area}(\omega(P)) = \frac{\sqrt{3}}{2} P^2$:

$$P(R) = \frac{2\sqrt{\pi}}{\sqrt[4]{3}} R. \tag{3.84}$$

And similarly for the square lattice, with $\mathrm{area}(\omega(P)) = P^2$:

$$P(R) = \sqrt{2\pi} R. \tag{3.85}$$

Thus, Equation 3.81 simplifies to:

$$R_0 = \min_R \frac{2\pi R h \sigma_{\mathrm{DW}}(\Delta_0(h)) + E_{\sigma\sigma,\mathrm{c}}(R, P(R))}{\mathrm{area}(\omega(P(R)))} \quad \Rightarrow \quad \frac{\partial}{\partial R} \frac{2\pi R h \sigma_{\mathrm{DW}} + E_{\sigma\sigma,\mathrm{c}}(R, P(R))}{R^2}\bigg|_{R=R_0} \overset{!}{=} 0, \tag{3.86}$$

with $P_0 = P(R_0)$, where $P(R)$ is given by Equation 3.85, and $\mathrm{area}(\omega(P(R))) \sim R^2$ for both square and hexagonal lattices. The first term in Equation 3.86 gives:

$$\frac{\partial}{\partial R} \frac{2\pi h \sigma_{\mathrm{DW}}}{R}\bigg|_{R=R_0} = -\frac{2\pi h \sigma_{\mathrm{DW}}}{R_0^2} \tag{3.87}$$

For the second term, the result depends on the lattice type.

First, consider the hexagonal lattice. The derivative of $E_{\sigma\sigma,\mathrm{c}}(R, P(R))$ in this case is given, for the limit $R_0/h \to \infty$, by the expansion:

$$\frac{\partial}{\partial R} \frac{E_{\sigma\sigma,\mathrm{c}}(R, P(R))}{R^2}\bigg|_{R=R_0} \overset{R_0/h\to\infty}{=} \mu_0 M_s^2 \left(2\frac{h^2}{R_0^2} \log\left(\frac{R_0}{h}\right) + c_{\infty,\mathrm{hex.}} \frac{h^2}{R_0^2} + \mathcal{O}\left(\left(\frac{h}{R_0}\right)^4\right)\right) \tag{3.88}$$

where $c_{\infty,\mathrm{hex.}}$ is given by

$$
\begin{aligned}
c_{\infty,\mathrm{hex.}} =& -3+3\log(4)-\frac{4756953416231377955074251 5}{3346212221363636162682421248\ 3^{3/4}\pi^{5/2}}-\frac{1898120687579670828272 65}{5666839779443574256435 2\sqrt[4]{3}\pi^{5/2}}\\
&+\frac{17536530812535204125}{3184707635509198848\sqrt[4]{3}\sqrt{7}\pi^{5/2}}-\frac{1886091771800191271017}{368934881474191032320\ 3^{3/4}\pi^{3/2}}\\
&-\frac{20225184484764247963259}{2178523581616950626746368 0\sqrt[4]{3}\pi^{3/2}}+\frac{6215247404955041\sqrt[4]{3}}{2369574133563392\sqrt{7}\pi^{3/2}}\\
&+\frac{46383575553517847149761497}{7863108552398681168412672 0\ 3^{3/4}\sqrt{\pi}}-\frac{5661888076505783777717}{1331624337820908257280\sqrt[4]{3}\sqrt{\pi}}\\
&+\frac{721890807924953}{148098383347712\sqrt[4]{3}\sqrt{7\pi}}\\
=&\,0.0479249
\end{aligned}
\tag{3.89}
$$

The first expression for $c_{\infty,\mathrm{hex.}}$, with the finite sum of terms, is exact, taking into account the orders considered in the multipole expansion and the Euler-Maclaurin expansion with $n = 5$. The large number of terms in the first expression of $c_{\infty,\mathrm{hex.}}$ arises from the calculation of $E_{\mathrm{c}\leftrightarrow\mathrm{c}}$ using the Euler-Maclaurin formula and the multipole expansion. The second expression is the numerical value of $c_{\infty,\mathrm{hex.}}$ up to 6 digits. Combining Equation 3.87 and Equation 3.88 results in:

$$
R_{0,\mathrm{hex.},R_0/h\to\infty}(h) = h\exp\left(-\frac{c_{\infty,\mathrm{hex.}}}{2}\right)\exp\left(\frac{\pi\sigma_{\mathrm{DW}}}{\mu_0 M_s^2 h}\right) = C_{\infty,\mathrm{hex.}}\,h\exp\left(\frac{\pi\sigma_{\mathrm{DW}}}{\mu_0 M_s^2 h}\right) = 0.976\,h\exp\left(\frac{\pi\lambda}{h}\right),
\tag{3.90}
$$

where $C_{\infty,\mathrm{hex.}} = \exp\left(-\frac{c_{\infty,\mathrm{hex.}}}{2}\right) = 0.976$. The convergence of $c_{\infty,\mathrm{hex.}}$ and $\exp\left(-\frac{c_{\infty,\mathrm{hex.}}}{2}\right)$ as the highest-order term of the multipole expansion, N, increases (as defined in Equation 3.50) is presented in Table S 2.

For the limit $R/h \to 0$, the derivative $E_{\sigma\sigma,\mathrm{c}}(R, P(R))$ is given by the expansion:

$$
\left.\frac{\partial}{\partial R}\frac{E_{\sigma\sigma,\mathrm{c}}(R,P(R))}{R^2}\right|_{R=R_0} \overset{R_0/h\to 0}{=} \mu_0 M_s^2\left(c_{0,\mathrm{hex.}}+\mathcal{O}\left(\left(\frac{R_0}{h}\right)^2\right)\right)
\tag{3.91}
$$

where $c_{0,\mathrm{hex.}}$ is given by

$$
\begin{aligned}
c_{0,\mathrm{hex.}} =& \frac{16}{3}+\frac{554486395121405\sqrt{\frac{\pi}{7}}}{87272261615616\ 3^{3/4}}+\frac{1886091771800191271017}{17708874310761169551 36\ 3^{3/4}\pi^{3/2}}\\
&+\frac{20225184484764247963259}{1045691319176136300838256 64\sqrt[4]{3}\pi^{3/2}}-\frac{31076237024775205}{18956593068507136\ 3^{3/4}\sqrt{7}\pi^{3/2}}\\
&-\frac{46383575553517847149761497}{1572621710479736233682534 40\ 3^{3/4}\sqrt{\pi}}+\frac{5661888076505783777717}{2663248675641816514560\sqrt[4]{3}\sqrt{\pi}}\\
&-\frac{3175592990259118017 25\sqrt{\pi}}{24967956334142029824\ 3^{3/4}}+\frac{3751753456667228838901 7027\sqrt{\pi}}{1228610711312293932564480 0\sqrt[4]{3}}\\
&-\frac{721890807924953}{296196766695424\sqrt[4]{3}\sqrt{7\pi}}\\
&+\frac{1}{2}\sqrt[4]{3}\sqrt{\pi}\log\left(4053+2340\sqrt{3}\right)+2\sqrt[4]{3}\sqrt{\pi}\log\left(53-20\sqrt{7}\right)\\
=&\,0.897651
\end{aligned}
\tag{3.92}
$$

Combining Equation 3.87 and Equation 3.91 results in

$$R_{0,\mathrm{hex.},R_0/h\to 0}(h) = \sqrt{\frac{2\pi}{c_{0,\mathrm{hex.}}}}\sqrt{\frac{h\sigma_{\mathrm{DW}}}{\mu_0 M_s^2}} = C_{0,\mathrm{hex.}}\sqrt{\frac{h\sigma_{\mathrm{DW}}}{\mu_0 M_s^2}} = 2.646\sqrt{\lambda h}, \tag{3.93}$$

where $C_{0,\mathrm{hex.}} = \sqrt{\frac{2\pi}{c_{0,\mathrm{hex.}}}} = 2.646$. The convergence of $c_{0,\mathrm{hex.}}$ and $\sqrt{\frac{2\pi}{c_{0,\mathrm{hex.}}}}$ as the highest considered order N of the multipole expansion increases is also shown in Table S 2.

The closed analytical formulae for both limits for the hexagonal lattice, shown in Figure S7 and Figure S8, demonstrate excellent agreement with the numerical minimizations.

N	1	3	5
$c_{\infty,\mathrm{hex.}}$	0.271945	0.103369	0.0479249
$C_{\infty,\mathrm{hex.}} = \exp\left(-c_{\infty,\mathrm{hex.}}/2\right)$	0.872867	0.949628	0.976322
$c_{0,\mathrm{hex.}}$	0.419062	0.862531	0.897651
$C_{0,\mathrm{hex.}} = \sqrt{2\pi/c_{0,\mathrm{hex.}}}$	3.87214	2.69900	2.64567

Table S 2: The numerical values of $c_{\infty,\mathrm{hex.}}$, $C_{\infty,\mathrm{hex.}} = \exp\left(-c_{\infty,\mathrm{hex.}}/2\right)$, $c_{0,\mathrm{hex.}}$, and $C_{0,\mathrm{hex.}} = \sqrt{2\pi/c_{0,\mathrm{hex.}}}$ for different highest-order term of the multipole expansion, N, (as defined in Equation 3.50). The Euler-Maclaurin formula was consistently applied with $n = 5$.

Now consider the square lattice: In this case, the derivative of $E_{\sigma\sigma,\mathrm{c}}(R, P(R))$ for the limit $R/h \to \infty$ is given by the expansion:

$$\frac{\partial}{\partial R}\frac{E_{\sigma\sigma,\mathrm{c}}(R,P(R))}{R^2}\bigg|_{R=R_0} \overset{R_0/h\to\infty}{=} \mu_0 M_s^2\left(2\frac{h^2}{R_0^2}\log\left(\frac{R_0}{h}\right) + c_{\infty,\mathrm{sq.}}\frac{h^2}{R_0^2} + \mathcal{O}\left(\left(\frac{h}{R_0}\right)^4\right)\right) \tag{3.94}$$

where $c_{\infty,\mathrm{sq.}}$ is given by

$$\begin{aligned}
c_{\infty,\mathrm{sq.}} =& -3 + 2\log(8) - \frac{74414433240160293094199038 5}{19807040628566084398385987584\pi^{11/2}} - \frac{385502348329329}{43980465111040\sqrt{2}\pi^{11/2}} \\
&+ \frac{13635213121172807 01}{16384000000000000\sqrt{10}\pi^{11/2}} - \frac{14552879810126559700740879}{309485009821345068724781056\pi^{9/2}} - \frac{1586140979577}{274877906944\sqrt{2}\pi^{9/2}} \\
&+ \frac{23657737229537733}{4096000000000000\sqrt{10}\pi^{9/2}} - \frac{21583254117230563988659 1}{36267774588438875241185 28\pi^{7/2}} - \frac{51814434133}{12884901888\sqrt{2}\pi^{7/2}} \\
&+ \frac{65631950658883}{15360000000000\sqrt{10}\pi^{7/2}} - \frac{691956617591009900705}{9444732965739290427392\pi^{5/2}} - \frac{205862455}{67108864\sqrt{2}\pi^{5/2}} \\
&+ \frac{221946424131}{64000000000\sqrt{10}\pi^{5/2}} - \frac{71204822310443233 37}{11068046444225730969 6\pi^{3/2}} - \frac{4388887}{1572864\sqrt{2}\pi^{3/2}} + \frac{32412507291}{10000000000\sqrt{10}\pi^{3/2}} \\
&+ \frac{51911722291897922441 5}{13316243378209082572 8\sqrt{\pi}} - \frac{5666967}{1261568\sqrt{2\pi}} + \frac{2821202491}{750000000\sqrt{10\pi}} \\
=& -0.037634
\end{aligned} \tag{3.95}$$

Combining Equation 3.87 and Equation 3.94 results in

$$R_{0,\mathrm{sq.},R_0/h\to\infty}(h) = h\exp\left(-\frac{c_{\infty,\mathrm{sq.}}}{2}\right)\exp\left(\frac{\pi\sigma_{\mathrm{DW}}}{\mu_0 M_s^2 h}\right) = C_{\infty,\mathrm{sq.}}\, h\exp\left(\frac{\pi\sigma_{\mathrm{DW}}}{\mu_0 M_s^2 h}\right) = 1.019\, h\exp\left(\frac{\pi\lambda}{h}\right), \tag{3.96}$$

where $C_{\infty,\text{sq.}} = \exp\left(-\frac{c_{\infty,\text{sq.}}}{2}\right) = 1.019$. The convergence of $c_{\infty,\text{sq}}$ and $\exp\left(-\frac{c_{\infty,\text{sq}}}{2}\right)$ as the highest order term of the multipole expansion increases, N, is shown in Table S 3.

And for the limit $R/h \to 0$, the derivative is given by the expansion.

$$\left.\frac{\partial}{\partial R}\frac{E_{\sigma\sigma,\text{c}}(R,P(R))}{R^2}\right|_{R=R_0} \overset{R_0/h\to 0}{=} \mu_0 M_s^2 \left(c_{0,\text{sq.}} + \mathcal{O}\left(\left(\frac{R_0}{h}\right)^2\right)\right) \tag{3.97}$$

where $c_{0,\text{sq.}}$ is given by

$$\begin{aligned}
c_{0,\text{sq.}} =& \frac{16}{3} + \frac{36936792469\sqrt{\frac{\pi}{10}}}{8662500000} - \frac{56350853\sqrt{\frac{\pi}{2}}}{5322240} + \frac{76229370433996265099 11889}{309485009821345068724781056 0\pi^{9/2}} \\
&+ \frac{830835751207}{2748779069440\sqrt{2}\pi^{9/2}} - \frac{12392148072615003}{40960000000000000\sqrt{10}\pi^{9/2}} + \frac{215832541172305639886591}{48357032784585166988247040\pi^{7/2}} \\
&+ \frac{51814434133}{171798691840\sqrt{2}\pi^{7/2}} - \frac{65631950658883}{204800000000000\sqrt{10}\pi^{7/2}} + \frac{968739264627413860987}{113336795588871485128704\pi^{5/2}} \\
&+ \frac{288207437}{805306368\sqrt{2}\pi^{5/2}} - \frac{517874989639}{1280000000000\sqrt{10}\pi^{5/2}} + \frac{35602411155221616685}{265633114661417543270 4\pi^{3/2}} \\
&+ \frac{21944435}{37748736\sqrt{2}\pi^{3/2}} - \frac{10804169097}{16000000000\sqrt{10}\pi^{3/2}} - \frac{51911722918979224415}{266324867564181651456\sqrt{\pi}} \\
&+ \frac{2819112479127893550 83\sqrt{\pi}}{133756908932903731200} + \frac{5666967}{2523136\sqrt{2\pi}} - \frac{2821202491}{1500000000\sqrt{10\pi}} \\
&+ \sqrt{2\pi}\log\left(644 - 288\sqrt{5}\right) + \sqrt{2\pi}\cosh^{-1}(99) \\
=& 0.943921
\end{aligned} \tag{3.98}$$

Combining Equation 3.87 and Equation 3.97 results in

$$R_{0,\text{sq.},R_0/h\to 0}(h) = \sqrt{\frac{2\pi}{c_{0,\text{hex.}}}}\sqrt{\frac{h\sigma_{\text{DW}}}{\mu_0 M_s^2}} = C_{0,\text{sq.}}\sqrt{\frac{h\sigma_{\text{DW}}}{\mu_0 M_s^2}} = 2.580\sqrt{\lambda h} \tag{3.99}$$

where $C_{0,\text{sq.}} = \sqrt{\frac{2\pi}{c_{0,\text{hex.}}}} = 2.580$. The values of $c_{0,\text{sq}}$ and $c_{0,\text{sq.}}$ show convergence as the highest order term of the multipole expansion, N, increases, as presented in Table S 3.

N	1	3	5	7	9	11
$c_{\infty,\text{sq.}}$	0.257892	0.0760682	0.0105734	−0.0176632	−0.0309894	−0.0376335
$C_{\infty,\text{sq.}} = \exp\left(-c_{\infty,\text{sq.}}/2\right)$	0.879021	0.962680	0.994727	1.00887	1.01562	1.01899
$c_{0,\text{sq.}}$	0.445089	0.895584	0.933464	0.941105	0.943223	0.943921
$C_{0,\text{sq.}} = \sqrt{2\pi/c_{0,\text{sq.}}}$	3.75722	2.64872	2.59443	2.58387	2.58097	2.58001

Table S 3: The numerical values of $c_{\infty,\text{sq.}}$, $C_{\infty,\text{sq.}} = \exp\left(-c_{\infty,\text{sq.}}/2\right)$, $c_{0,\text{sq.}}$, and $C_{0,\text{sq.}} = \sqrt{2\pi/c_{0,\text{sq.}}}$ for different highest-order term of the multipole expansion, N, (as defined in Equation 3.50). The Euler-Maclaurin formula was consistently applied with $n = 5$.

For both the square and hexagonal lattices, the formulae for the equilibrium radius are given by $R_{0,R_0/h\to\infty}(h) = C_\infty h \exp\left(\frac{\pi\lambda}{h}\right)$ and $R_{0,R_0/h\to 0}(h) = C_0\sqrt{\lambda h}$. The minimal difference between these two solutions occurs at $\frac{\lambda}{h} \approx \frac{1}{6}$. Therefore, there is the regime $\frac{\lambda}{h} \gg \frac{1}{6}$ (towards thin films), where the relation $R_{0,R_0/h\to\infty}(h) = C_\infty h \exp\left(\frac{\pi\lambda}{h}\right)$ holds, and the regime $\frac{\lambda}{h} \ll \frac{1}{6}$ (towards thick

films), where $R_{0,R_0/h\to 0}(h) = C_0\sqrt{\lambda h}$ is valid. The closed-form analytical solutions for both limits of the hexagonal and square lattice, as it will be shown in Figure S7 and Figure S8, align very well with the numerical minimizations. It can be observed that the formulae provide a good approximation within the respective regimes, even not far from $\frac{\lambda}{h} = \frac{1}{6}$. The threshold between the regimes $\frac{\lambda}{h} = \frac{1}{6}$ corresponds to $n_r = 30$ in our specific system. A classification of two regimes with different scaling based on λ/h has already been reported for stripe domain systems in Ref. 15.

3.9.2 Numerical result

Using our closed analytical description, we will show now our numerical results. To obtain the lattice configuration (R, P) with the lowest energy for arbitrary h, beyond the two mentioned limits ($R_0/h \to 0$, $R_0/h \to \infty$), R_0 and P_0 are determined through numerical minimization. This is done using Equation 3.78, with $B_z = 0$, meaning the Zeeman energy vanishes ($E_\mathrm{Z} = 0$). The functional relationship of the dimensionless quantity $\frac{R_0}{h}$ and $\frac{P_0}{h}$ as a function of the dimensionless quantity $\frac{\sigma_\mathrm{DW}}{h\mu_0 M_s^2} = \frac{\lambda}{h}$ is determined through numerical minimization for the hexagonal and square lattice, i.e., $\left(\frac{P_0}{h}\right)\left(\frac{\lambda}{h}\right)$ and $\left(\frac{R_0}{h}\right)\left(\frac{\lambda}{h}\right)$. There is only a 3% deviation in the ratios $R_0\left(\frac{\lambda}{h}\right)/P_0\left(\frac{\lambda}{h}\right)$ from the analytical ratios assuming charge neutrality, see Equation 3.84 and Equation 3.85. Additionally, we calculated the areal energy density ϵ (Equation 3.72) using our numerical results of $R_0(\lambda/h)$ and $P_0(\lambda/h)$ for both hexagonal and square lattices. We found that

$$\epsilon_\mathrm{hex.}(R_{0,\mathrm{hex.}}(\lambda/h), P_{0,\mathrm{hex.}}(\lambda/h)) < \epsilon_\mathrm{sq.}(R_{0,\mathrm{sq.}}(\lambda/h), P_{0,\mathrm{sq.}}(\lambda/h)), \tag{3.100}$$

which is evident since the hexagonal lattice has a higher packing density.

The result of $\left(\frac{R_0}{h}\right)\left(\frac{\lambda}{h}\right)$ for the hexagonal lattice is shown in Figure S7. Also shown are the closed analytical formulae from the previous section for the limits $R_0/h \to 0$ and $R_0/h \to \infty$, where agreement is observed in the respective limits.

Additionally, $R_0(h)$, with $\sigma_\mathrm{DW} = \sigma_\mathrm{DW}(\Delta_0(h))$, $\Delta_0(h)$ determined as described before, is explicitly plotted in Figure S8 for square (orange) and hexagonal (blue) lattices. We have also included the results for micromagnetic simulations assuming an hexagonal lattice with and without applying the effective medium model (green and pink dots, respectively). The good agreement with the closed analytical formulae and numerical micromagnetic simulations is visible.

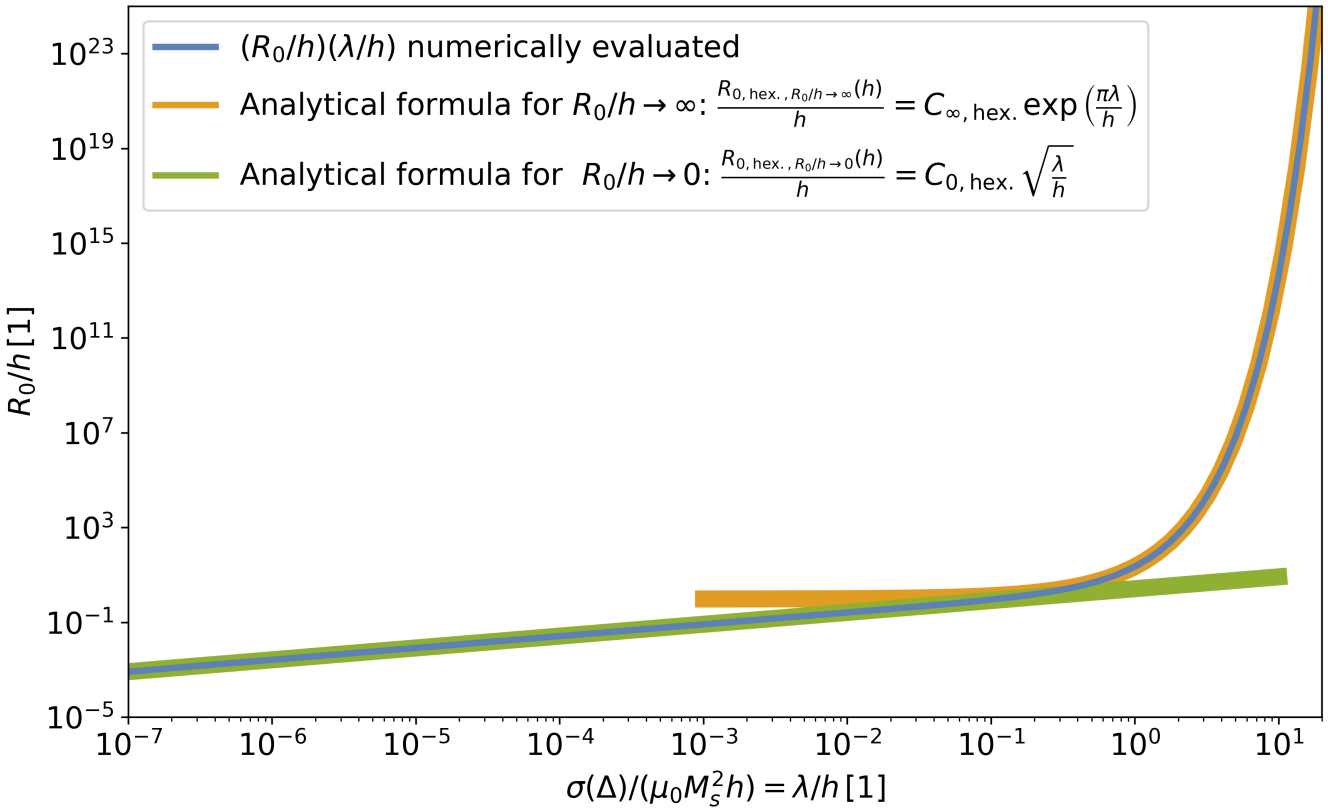

Figure S 7: Functional relationship between the dimensionless quantities $\frac{R_0}{h}$ and $\frac{\sigma_{\text{DW}}}{h\mu_0 M_s^2} = \frac{\lambda}{h}$, i.e., $\left(\frac{R_0}{h}\right)\left(\frac{\sigma_{\text{DW}}}{h\mu_0 M_s^2}\right) = \left(\frac{R_0}{h}\right)\left(\frac{\lambda}{h}\right)$ for the hexagonal lattice. The numerical minimization and the analytical formulae for the limits are shown.

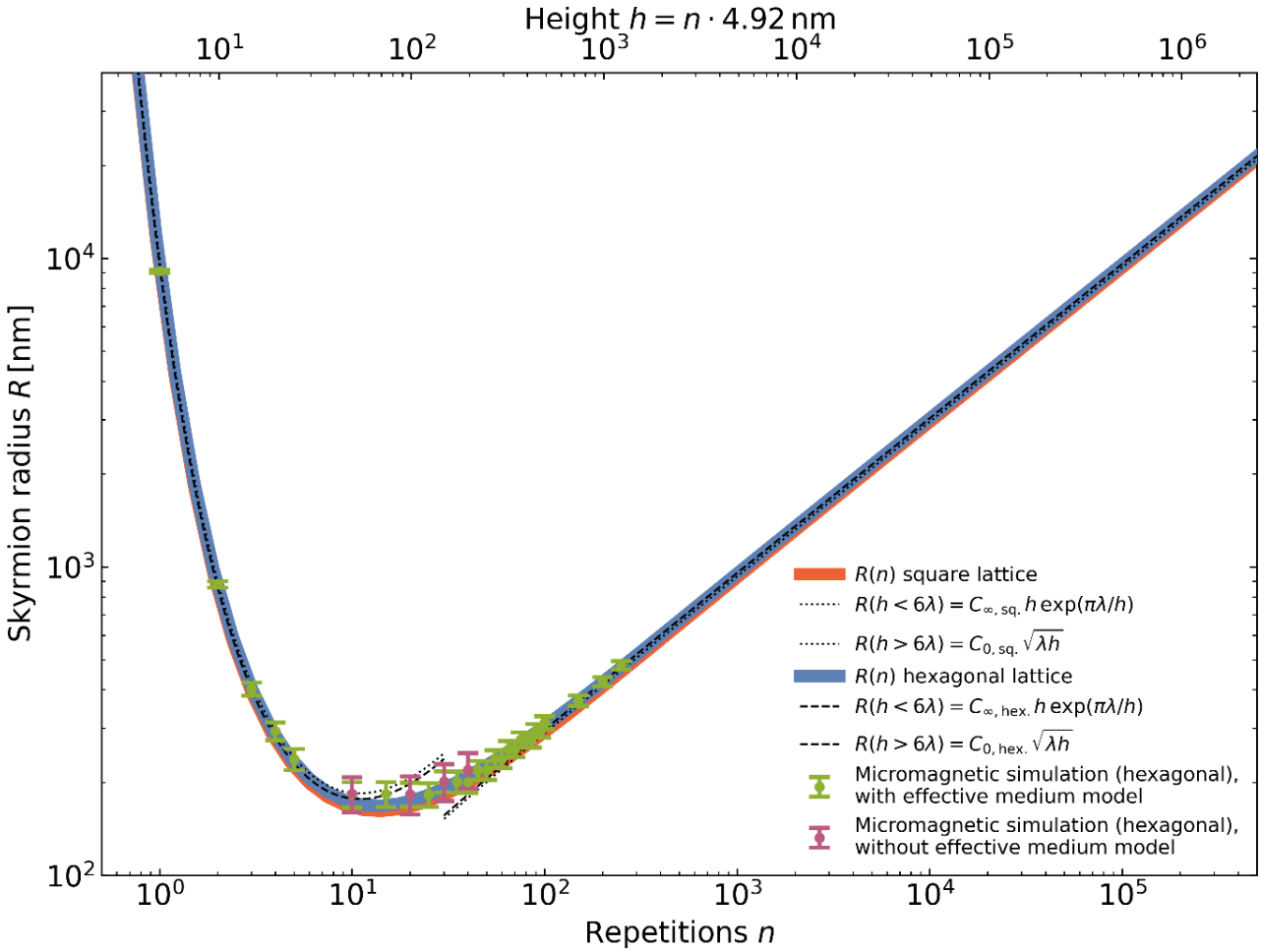

Figure S 8: Results of the skyrmion lattice model: Orange represents the square lattice, while blue, the hexagonal arrangement. We also include the closed-form analytical limit formulae for the hexagonal lattice (dashed line) and the square lattice (dotted line). Note that R_0 is referred to simply as R, as R_0 represents the radius with the lowest energy density. The plot focuses exclusively on the stable configurations, where the radius R equals R_0. Green and purple dots represent the micromagnetic simulation results for hexagonal lattice with and without using the effective medium model. Error bars indicate the estimate of the simulation accuracy resulting from the finite domain wall width and discretization. Both results are compatible within the given uncertainty.

3.10 Determination of the equilibrium values of R and P with external field $B_z \neq 0$

To obtain the lattice configuration (R, P) with the lowest energy for arbitrary h, with an external Zeeman field B_z, R_0 and P_0 are determined through numerical minimization. For this, Equation 3.78 is used, and the functions $\left(\frac{R_0}{h}\right)\left(\frac{\lambda}{h}, B_z\right)$ and $\left(\frac{P_0}{h}\right)\left(\frac{\lambda}{h}, B_z\right)$ are numerically determined for the case of $n_r = 15$, giving:

$$\frac{\lambda}{h} = \frac{\sigma(\Delta_0(n_r h_{\mathrm{sr}}), n_r h_{\mathrm{sr}})}{\mu_0 M_s^2 n_r h_{\mathrm{sr}}} = 0.297, \tag{3.101}$$

with $\Delta_0(h)$ from Equation 3.80. The result, explicitly solved for $R(B_z)$ after minimization (instead of $(R/h)(B_z)$), is shown in Figure S9. Similar behavior has been previously observed for

domain walls[17].

When the field is aligned with the skyrmions ($B_z < 0$), both the periodicity and the skyrmion radius increase. The curve ends when $P = R/2$, at which point the model breaks down, as the skyrmions significantly deform away from a cylindrical shape.

In the case that the field is opposite to the skyrmion core direction ($B_z > 0$), the skyrmions shrink, the periodicity first slightly decreases and then increases, diverging at $B_{z,0} \approx 30.92\,\mathrm{mT}$ with $P(B_z) \sim (B_z - B_{z,0})^{-\alpha}$, where $\alpha = 0.33 \approx 1/3$ (for square and hexagonal lattices). The skyrmion radius remains finite. Since the periodicity diverges, this is the limit of an isolated skyrmion. Therefore, for $B > B_{z,0}$, we numerically minimize the energy of an isolated skyrmion, *i.e.*,

$$R_0 = \arg\min_R \left[2\pi R h \sigma_{\mathrm{DW}}(\Delta_0) + E_{\mathrm{c}}(R) + E_{\mathrm{c}\leftrightarrow\mathrm{f}}(R) + E_{\mathrm{Z}}(R)\right], \tag{3.102}$$

the result is also shown in Figure S9. Agreement can be observed in the transition from the skyrmion lattice to the isolated skyrmion. An analytical solution for $R_0(B_Z)$ from Equation 3.102 can be given in the limit $R/h \to \infty$ as an approximation for $R_0(B_z)$:

$$R_0(h) = -\frac{hM_s\mu_0}{2\pi B_z} W_{-1}\left(-\frac{\pi B_z}{4M_s\mu_0}\exp\left(\frac{\pi\sigma_{\mathrm{DW}}}{h\mu_0 M_s^2} - \frac{1}{2}\right)\right), \tag{3.103}$$

where W_{-1} is the Lambert W function on the -1 branch, and this function is also shown in Figure S9.

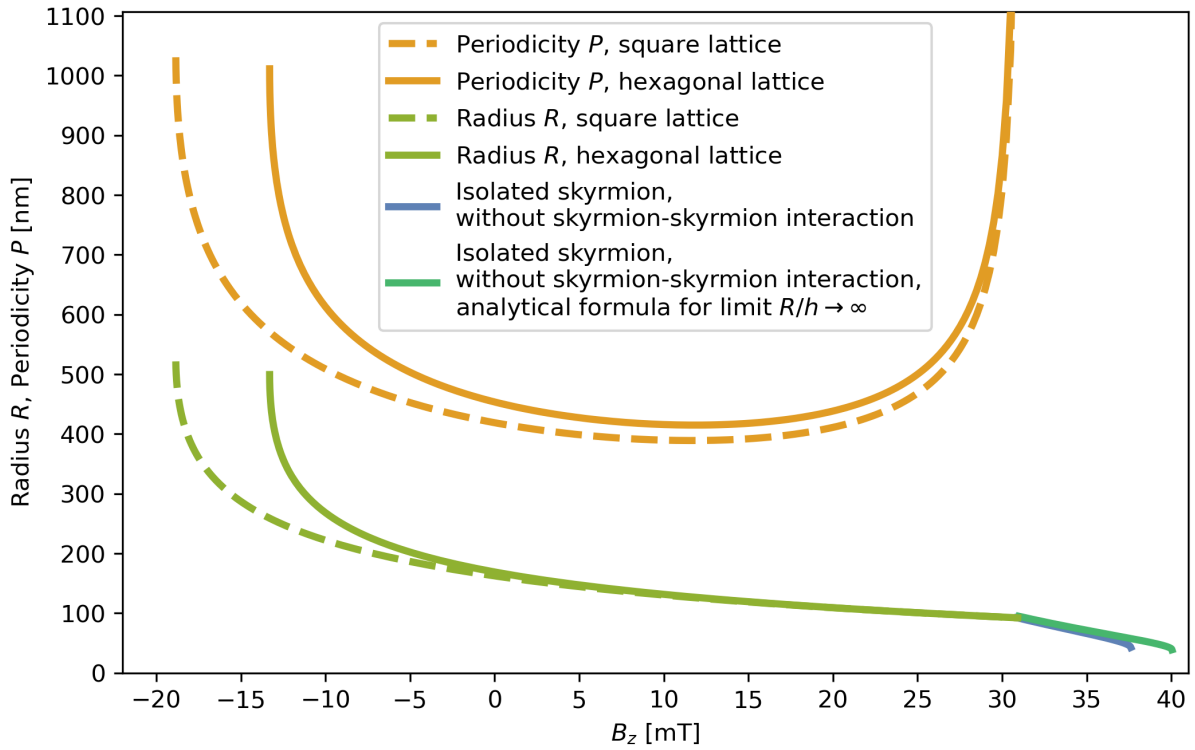

Figure S 9: Dependence of the skyrmion lattice with periodicity P and radius R on the external field B_{ext} (along the z-direction) for square and hexagonal lattices for $n_r = 15$ repetitions. At $B_z = 30.92\,\mathrm{mT}$, the periodicity diverges, and the system transitions effectively to the case of an isolated skyrmion lattice. Therefore, the analytical solutions (in the limit $R/h \to \infty$) and numerical for an isolated skyrmion under an external field B_z are also plotted for $B_z > 30.92\,\mathrm{mT}$.

Note S.4 Micromagnetic simulations

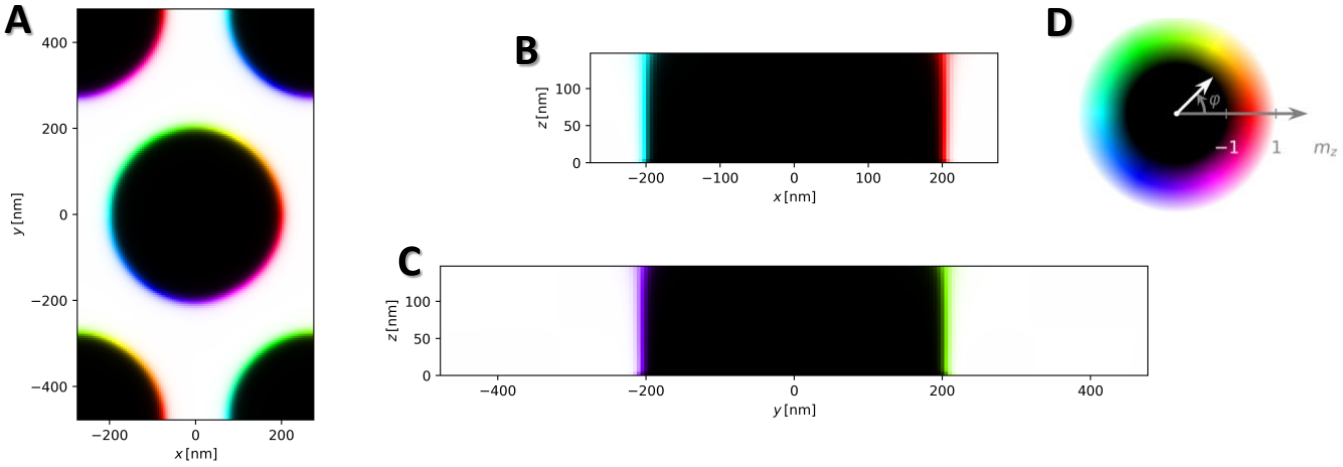

Figure S 10: Minimized magnetization configuration, with the periodicity corresponding to the lowest energy density for $n_r = 30$ in a hexagonal lattice. The considered unit cell ω, along with a quarter of each of four adjacent unit cells are simulated. The plots show the magnetization configuration in **(A)** the xy-plane, **(B)** the xz-plane, and **(C)** the yz-plane. **(D)** The color wheel illustrates the magnetization orientation used in the plots, highlighting the Néel character of the walls.

The micromagnetic simulations were performed using MuMax^3 [8]. Discretization in the x and y directions was done using a cell size of $5\,\mathrm{nm}$. The hexagonal lattice (rather than the square lattice, as the hexagonal lattice has a higher packing density) was simulated with the considered unit cell ω along with a quarter of each of the four adjacent unit cells, so that the region $\{(x, y) \in \mathbb{R}^2 || x| \leq P/2, |y| \leq \sqrt{3}P/2\}$ was simulated, as it can be seen in Figure S10. Periodic boundary conditions are applied in both the x and y directions, with 30 repetitions of the demagnetizing kernel in the positive and negative x and y directions, respectively.

For a group of simulations, the effective medium model was used, and the cell height in the z-direction was set to $h = n_r h_{\mathrm{sr}}$. For repetitions $n_r > 1$, different periodicities P spaced apart by a step size of $50\,\mathrm{nm}$ were simulated with the skyrmion lattice Ansatz Equation 3.11 as the initial configuration, followed by minimization of the total energy using the steepest conjugate gradient method[18]. The areal total energy density ϵ for different values of P at the same height h was compared, and the periodicity corresponding to the smallest energy density ϵ was selected, which was used as P_0. From the magnetically minimized configuration at P_0, the skyrmion radius R_0 was determined from the magnetization using $R_0 = R_{\mathrm{est.}}(m_t = 0)$, where $R_{\mathrm{est.}}(m_t)$ is defined as:

$$R_{\mathrm{est.}}(m_t) = \sqrt{\frac{1}{\pi}\int_\Omega \mathrm{d}^2\vec{r} \begin{cases} 1 & \text{if } m_z(\vec{r}) \leq m_t \\ 0 & \text{otherwise} \end{cases}}. \tag{4.1}$$

Error bars for R_0 were determined from the configuration at P_0 as $\pm\frac{1}{2} \times [R_{\mathrm{est.}}(m_t^+) - R_{\mathrm{est.}}(m_t^-)]$, with $(m_t^\pm = \pm 0.95)$.

In the case of one repetition $n_r = 1$, the skyrmion lattice ansatz shown in Equation 3.12 was used, and P and R were independently varied step by step (the step size of P was $2.5\,\mu\mathrm{m}$, and the step size of R was varied between $20\,\mathrm{nm}$ and $150\,\mathrm{nm}$), being the energy calculated at

each step. Note the different approach followed in this calculation compared to the previous one, when the vector field within all discretized magnetization cells was minimized, for the sake of computational costs. Δ_0 was obtained using Equation 3.80, while R_0 and P_0 were determined from the configuration with the lowest total areal energy density. Error bars in this case are calculated from the step size used when varying R and P. In all these simulations, the ratio R_0/P_0 deviated by at most 2% from the analytical ratio obtained from Equation 3.84. The results from our micromagnetic simulations are shown in Figures S 8 and S 10.

In addition, a number of simulations was conducted without using the effective medium model, *i.e.*, each magnetic layer was resolved and computed individually. The non-magnetic layers were not simulated, only the magnetic ones. Thus, the cell size in the z-direction is $0.86\,\mathrm{nm}$, being the spacing between the cells of $4.92\,\mathrm{nm}$, reproducing the experimental system. The MuMax^3 code was adjusted for this, particularly for the calculation of the demagnetization kernel in MuMax^3 (verified with the standard version of MuMax^3 for specific systems). The skyrmion radius R was determined using $R_{\mathrm{est.}}(0)$ for each layer and averaged. Error bars were calculated by layer-wise determination of $R_{\mathrm{est.}}(0.95)$ and $R_{\mathrm{est.}}(-0.95)$. The maximum value of $R_{\mathrm{est.}}(0.95)$ minus the minimum value of $R_{\mathrm{est.}}(-0.95)$, divided by 2, was used as the error. The relative deviation of R, determined using $R_{\mathrm{est.}}(0)$, from the mean across the layers is less than 1%. The deviation from the respective mean values for the upper threshold $R_{\mathrm{est.}}(0.95)$ and lower threshold $R_{\mathrm{est.}}(-0.95)$ is less than 7%. The results were already included in Figure 2 of the main text and in Figure S8. Our results evidence the good agreement between the simulations with and without the effective medium model, which validates its use. This reduces notably the computational costs of the simulations.

For the other simulations in the main text, MuMax^3 was also used, with a discretization cell size of $5\,\mathrm{nm}$ in the x and y directions. The effective medium model was applied, and the energy was minimized using the steepest conjugate gradient method[18].

Supplemental References

1. Inc., W. R. Mathematica, Version 14.1 (2024). Champaign, IL.

2. Rich, A., Scheibe, P., and Abbasi, N. (2018). Rule-based integration: An extensive system of symbolic integration rules. Journal of Open Source Software *3*, 1073.

3. Virtanen, P., Gommers, R., Oliphant, T. E., Haberland, M., Reddy, T., Cournapeau, D., Burovski, E., Peterson, P., Weckesser, W., Bright, J., van der Walt, S. J., Brett, M., Wilson, J., Millman, K. J., Mayorov, N., Nelson, A. R. J., Jones, E., Kern, R., Larson, E., Carey, C. J., Polat, İ., Feng, Y., Moore, E. W., VanderPlas, J., Laxalde, D., Perktold, J., Cimrman, R., Henriksen, I., Quintero, E. A., Harris, C. R., Archibald, A. M., Ribeiro, A. H., Pedregosa, F., van Mulbregt, P., Vijaykumar, A., Bardelli, A. P., Rothberg, A., Hilboll, A., Kloeckner, A., Scopatz, A., Lee, A., Rokem, A., Woods, C. N., Fulton, C., Masson, C., Häggström, C., Fitzgerald, C., Nicholson, D. A., Hagen, D. R., Pasechnik, D. V., Olivetti, E., Martin, E., Wieser, E., Silva, F., Lenders, F., Wilhelm, F., Young, G., Price, G. A., Ingold, G.-L., Allen, G. E., Lee, G. R., Audren, H., Probst, I., Dietrich, J. P., Silterra, J., Webber, J. T., Slavič, J., Nothman, J., Buchner, J., Kulick, J., Schönberger, J. L., de Miranda Cardoso, J. V., Reimer, J., Harrington, J., Rodríguez, J. L. C., Nunez-Iglesias, J., Kuczynski, J., Tritz, K., Thoma, M., Newville, M., Kümmerer, M., Bolingbroke, M., Tartre, M., Pak, M., Smith, N. J., Nowaczyk,

N., Shebanov, N., Pavlyk, O., Brodtkorb, P. A., Lee, P., McGibbon, R. T., Feldbauer, R., Lewis, S., Tygier, S., Sievert, S., Vigna, S., Peterson, S., More, S., Pudlik, T. et al. (2020). Scipy 1.0: fundamental algorithms for scientific computing in python. Nature Methods *17*, 261–272.

4. Woo, S., Litzius, K., Krüger, B., Im, M.-Y., Caretta, L., Richter, K., Mann, M., Krone, A., Reeve, R. M., Weigand, M. et al. (2016). Observation of room-temperature magnetic skyrmions and their current-driven dynamics in ultrathin metallic ferromagnets. Nature Materials *15*, 501–506.

5. Romming, N., Kubetzka, A., Hanneken, C., von Bergmann, K., and Wiesendanger, R. (2015). Field-dependent size and shape of single magnetic skyrmions. Physical Review Letters *114*, 177203.

6. Boulle, O., Vogel, J., Yang, H., Pizzini, S., de Souza Chaves, D., Locatelli, A., Menteş, T. O., Sala, A., Buda-Prejbeanu, L. D., Klein, O. et al. (2016). Room-temperature chiral magnetic skyrmions in ultrathin magnetic nanostructures. Nature Nanotechnology *11*, 449–454.

7. Büttner, F., Lemesh, I., and Beach, G. S. (2018). Theory of isolated magnetic skyrmions: From fundamentals to room temperature applications. Scientific reports *8*, 4464.

8. Vansteenkiste, A., Leliaert, J., Dvornik, M., Helsen, M., Garcia-Sanchez, F., and Van Waeyenberge, B. (2014). The design and verification of MuMax3. AIP Advances *4*, 107133.

9. Cortés-Ortuño, D., Beg, M., Nehruji, V., Breth, L., Pepper, R., Kluyver, T., Downing, G., Hesjedal, T., Hatton, P., Lancaster, T., Hertel, R., Hovorka, O., and Fangohr, H. (2018). Proposal for a micromagnetic standard problem for materials with dzyaloshinskii–moriya interaction. New Journal of Physics *20*, 113015.

10. Cape, J. A., and Lehman, G. W. (1971). Magnetic Domain Structures in Thin Uniaxial Plates with Perpendicular Easy Axis. Journal of Applied Physics *42*, 5732–5756.

11. Lorenz, L. (1879). Ueber die Fortpflanzung der Electricität. Annalen der Physik *243*, 161–193.

12. Ostrowski, A. (1969). On the remainder term of the euler-maclaurin formula. Journal für die reine und angewandte Mathematik *0239-0240*, 268–286.

13. Lemesh, I., Büttner, F., and Beach, G. S. D. (2017). Accurate model of the stripe domain phase of perpendicularly magnetized multilayers. Phys. Rev. B *95*, 174423.

14. Büttner, F., Krüger, B., Eisebitt, S., and Kläui, M. (2015). Accurate calculation of the transverse anisotropy of a magnetic domain wall in perpendicularly magnetized multilayers. Phys. Rev. B *92*, 054408.

15. Kaplan, B., and Gehring, G. (1993). The domain structure in ultrathin magnetic films. Journal of Magnetism and Magnetic Materials *128*, 111–116.

16. Kittel, C. (1946). Theory of the structure of ferromagnetic domains in films and small particles. Phys. Rev. *70*, 965–971.

17. Kooy, C. (1960). Experimental and theoretical study of the domain configuration in thin layers of $BaFe_{12}$ O_{19}. Philips Res. Repts *15*.

18. Exl, L., Bance, S., Reichel, F., Schrefl, T., Peter Stimming, H., and Mauser, N. J. (2014). Labonte's method revisited: An effective steepest descent method for micromagnetic energy minimization. Journal of Applied Physics *115*.